Covariation of Airborne Biogenic Tracers (CO_2, COS, and CO) Supports Stronger Than Expected Growing Season Photosynthetic Uptake in the Southeastern US

Nicholas C. Parazoo[1] , **Kevin W. Bowman[1]** , **Bianca C. Baier[2,3]** , **Junjie Liu[1]** , **Meemong Lee[1]** , **Le Kuai[1]** , **Yoichi Shiga[4]** , **Ian Baker[5]** , **Mary E. Whelan[6]** , **Sha Feng[7,8]** , **Maarten Krol[9,10]** , **Colm Sweeney[3]** , **Benjamin R. Runkle[11]** , **Elahe Tajfar[11]**, and **Kenneth J. Davis[7,8]**

[1]Jet Propulsion Laboratory, California Institute of Technology, Pasadena, CA, USA, [2]Cooperative Institute for Research in Environmental Sciences, University of Colorado-Boulder, Boulder, CO, USA, [3]NOAA Earth System Research Laboratory Global Monitoring Division, Boulder, CO, USA, [4]Universities Space Research Association, Moffett Field, CA, USA, [5]Cooperative Institute for Research in the Atmosphere, Colorado State University, Fort Collins, CO, USA, [6]Department of Environmental Sciences, Rutgers, The State University of New Jersey, New Brunswick, NJ, USA, [7]Department of Meteorology and Atmospheric Science, Pennsylvania State University, University Park, PA, USA, [8]Earth and Environmental Systems Institute, Pennsylvania State University, University Park, PA, USA, [9]Institute for Marine and Atmospheric Research, Utrecht University, Utrecht, The Netherlands, [10]Meteorology and Air Quality, Wageningen University & Research, Wageningen, The Netherlands, [11]Department of Biological and Agricultural Engineering, The University of Arkansas, Fayetteville, AR, USA

Abstract The Atmospheric Carbon Transport (ACT)-America Earth Venture mission conducted five airborne campaigns across four seasons from 2016 to 2019, to study the transport and fluxes of Greenhouse gases across the eastern United States. Unprecedented spatial sampling of atmospheric tracers (CO_2, carbon monoxide [CO], carbonyl sulfide [COS]) related to biospheric processes offers opportunities to improve our qualitative and quantitative understanding of seasonal and spatial patterns of biospheric carbon uptake. Here, we examine co-variation of boundary layer enhancements of CO_2, CO, and COS across three diverse regions: the crop-dominated Midwest, evergreen-dominated South, and deciduous broadleaf-dominated Northeast. To understand the biogeochemical processes controlling these tracers, we compare the observed co-variation to simulated co-variation resulting from model- and satellite- constrained surface carbon fluxes. We found indication of a common terrestrial biogenic sink of CO_2 and COS and secondary production of CO from biogenic sources in summer throughout the eastern US, driven by stomatal conductance. Upper Midwest crops drive ΔCO_2 and ΔCOS depletion from early to late summer. Northeastern temperate forests drive ΔCO_2 and ΔCOS depletion in late summer. The unprecedented ACT-America flask samples uncovered evidence that southern humid temperate forests photosynthesize and absorb CO_2 and COS, and emit CO precursors, deep into the growing season. Satellite- constrained carbon fluxes capture much of the observed seasonal and spatial variability, but underestimate the magnitude of net CO_2 and COS depletion in the South, indicating a stronger than expected net sink of CO_2 in late summer. Additional sampling of the South will more accurately constrain underlying biological processes and climate sensitivities governing southern carbon dynamics.

Plain Language Summary The Atmospheric Carbon Transport (ACT)-America airborne mission provided unprecedented sampling of atmospheric greenhouse gas concentrations throughout the eastern United States from 2016 to 2019. A subset of these gases, namely carbon dioxide (CO_2), carbonyl sulfide (COS), and carbon monoxide (CO), are strongly influenced by photosynthetic activity in plants. Unlike other sources of carbon such as fossil fuels and biomass burning, photosynthetic influences on CO_2, COS, and CO are correlated in time and space. As such, the covariation of boundary layer enhancements of CO_2, COS, and CO can provide clues about the seasonal and spatial distribution of plant carbon uptake. By examining this covariation across diverse regions in the eastern US, we uncovered evidence that humid temperate forests in the previously poorly constrained southern US continue to photosynthesize and absorb CO_2 and COS (and emit CO through biogenic volatile organic compound precursor emissions) deeper into the growing season than expected by models and satellite-constrained

estimates. Our results imply that southern US forests have stronger climate sensitivities than currently accounted for in models.

1. Introduction

The global terrestrial biosphere removes 20% of fossil emissions from the atmosphere (Arneth et al., 2017). The exact spatial distribution and underlying drivers of the increase in the terrestrial carbon sink has been a matter of debate for decades, but it is generally agreed to be split between the tropics and northern extra-tropics and driven by a combination of nutrient (CO_2, N) fertilization, thermal fertilization, and land cover/land use change (Liu, Wennberg, et al., 2020; Madani et al., 2020; Schimel et al., 2015; Stephens et al., 2007). Global top-down inversion studies leveraging surface-based CO_2 stations in northern latitudes (CarbonTracker, CT2019) indicate strong and persistent CO_2 uptake in North America (NA) of ∼0.6 Pg C from 2001 to 2018 (https://www.esrl.noaa.gov/gmd/ccgg/carbontracker/), driven by temperate ecosystems in the eastern US (east of the Rockies) and in southern Canada (Peters et al., 2007). Recent inversion efforts that incorporate satellite-based CO_2 observations support these estimates for temperate eastern North America, showing a statistically significant sink of similar magnitude (∼0.5 Pg C) over the period 2010–2018 (Liu, Baskaran, et al., 2020). These results are encouraging as we move toward combined surface- and satellite-based inversion approaches to improve spatially and temporally integrated constraints of net CO_2 exchange at regional and global scales, and advance regional-scale understanding of terrestrial CO_2 sinks (e.g., Byrne, Liu, Bloom, et al., 2020; Byrne, Liu, Lee, et al., 2020).

Airborne strategies focused on multi-tracer vertical profiles within continental interiors offer additional opportunities for studying spatially variable sources and sinks. Intensive airborne campaigns enable long-distance transect flights needed to sample multiple air masses across biologically diverse regions, sometimes multiple times per day, at spatial scales ranging from 100 to 1,000 km. Moreover, airborne campaigns that fly into and out of the atmospheric boundary layer can sample air immediately in contact with the surface for increased sensitivity to local processes, as well as provide periodic sampling of background air in the free troposphere, thus accounting for the influence of long-range transport (Baier et al., 2020; Parazoo et al., 2016). These flight strategies provide a critical advantage over column integrated satellite data, and fixed-point tower data, by directly measuring spatial gradients in anthropogenic and biogenic land surface influence.

Key to disentangling multiple anthropogenic and biogenic CO_2 sources and sinks (agricultural activity, forest productivity, biomass burning, gas and oil extraction and consumption) is multi-species sampling. Atmospheric carbon monoxide (CO) and carbonyl sulfide (COS) are increasingly being utilized to track biogenic activity and gross primary productivity (GPP; Campbell et al., 2008; Hudman et al., 2008). Plant uptake of atmospheric CO_2 and COS are directly related to photosynthesis through stomatal conductance (Berry et al., 2013; Campbell et al., 2008). While the main source of atmospheric CO is incomplete combustion of biomass and fossil fuel, and subsequent oxidation of hydrocarbons, a nontrivial secondary source is biogenic volatile organic compounds (BVOCs) emitted from vegetation, which oxidize to produce CO accounting for ∼18% of the global CO budget (Worden et al., 2019). In the absence of biomass burning and continued CO emissions from anthropogenic sources, the relative importance of secondary CO production increases.

Airborne COS and CO observations provide a unique opportunity to more directly study biogeochemical processes related at multiple temporal and spatial scales. Boundary layer CO data collected during the ICARTT aircraft campaign in the eastern US in summer 2004 revealed strong emissions from isoprene sources centered in the Southeast US, which exceeded regionally integrated anthropogenic emissions that peak in the Northeast near the strongest combustion sources (Hudman et al., 2008). Vertical COS profiles collected from the NOAA/Global Monitoring Laboratory (GML) light aircraft network from 2005 to 2012 indicate a hotspot of growing season GPP arising from intense agricultural activity in the upper Midwest US, exceeding all other regions in the US (Hilton et al., 2017). This hotspot is consistent with satellite-based measurements of solar induced fluorescence (SIF), another important signal of biogenic activity and in particular the light reactions of photosynthesis (Guanter et al., 2014). Crops are also implicated in the large seasonal, regional depletion in BL CO_2 observed by towers (Miles et al., 2012) and the large net annual

CO_2 fluxes inferred from those tower data (Schuh et al., 2013). Ecosystem model simulations of GPP show a range of spatial patterns in the eastern US, and only a subset of models are consistent with strong crop uptake in the Midwest inferred from SIF and COS (Guanter et al., 2014; Hilton et al., 2017). Multi-tracer data thus provide important proxies for studying spatial GPP variability, and offer unique benchmarks for improving model formulations of agricultural productivity, light capture by leaves, and CO_2 diffusion by stomatal conductance (Hilton, 2018; Whelan et al., 2020).

Atmospheric Carbon and Transport (ACT)-America, is a NASA Earth Venture Suborbital airborne mission that targeted multi-species vertical profiles in the eastern US for improved understanding of CO_2 sources and sinks (Davis et al., 2021; Wei et al., 2021). ACT-America conducted five airborne campaigns across four seasons from 2016 to 2019, capturing vertical gradients of CO_2, CO, and COS across three unique regions including the humid sub-tropical, evergreen-dominated South, seasonally warm- to hot- crop-dominated Midwest, and the warm temperate, deciduous broadleaf forest dominated Northeast. A subset of ACT-America flights were coordinated with satellite overpasses from the Orbiting Carbon Observatory (OCO-2), providing simultaneous measurements of column-integrated atmospheric CO_2 and underlying SIF. The combination of ACT-America, OCO-2, and existing airborne measurement networks from NOAA/GML (Sweeney et al., 2015) provides an unprecedented wealth of information about biological processes driving CO_2 uptake across the central and eastern US.

Here, we present a first interpretation of ACT-America tracer-tracer distributions, and their co-variation, across the central and eastern US. We focus on three biologically sensitive tracer species (CO_2, CO, and COS), which are collected periodically in airborne flask samples (~10–50 samples per region and campaign), and co-analyzed in the laboratory, providing high precision measurements collocated in space and time. We analyze observed and predicted seasonal distributions of individual species, and their covariation, across the three ACT regions to gain a better understanding of the seasonal and spatial distribution of net CO_2 sources and sinks, and the underlying biogenic and anthropogenic drivers.

This study has three main objectives: (a) first interpretation of ACT-America tracer-tracer covariation, (b) examination of underlying surface flux drivers across diverse regions in the central and eastern US, and (c) evaluation of observed versus expected surface flux patterns, providing insight into processes that are missing from models. We accomplish these objectives in three main steps: (a) Establish observed correlation patterns between CO_2, CO, and COS (Section 2.1), (b) Provide satellite constrained estimates of surface fluxes of CO_2, CO, and COS accounting for multiple carbon sources and sinks including terrestrial and oceanic biological exchange, biomass burning and anthropogenic emissions (Section 2.2), (c) Convolve posterior surface fluxes with surface influence functions for attribution of observed correlation patterns (Section 2.3). We also use simulation experiments to evaluate the use of airborne free troposphere data to account for background influences from boundary layer data (Text S1). By using a model-data analysis framework, this study provides a deeper investigation into the processes driving observed CO_2 patterns.

2. Methods

2.1. ACT-America Tracer Observations

High quality CO_2, CO, and COS trace gas mole fractions were collected *in situ* from two instrumented aircraft platforms, the NASA Langley Beechcraft B200 King Air and the NASA Goddard Space Flight Center's C-130 Hercules (Davis et al., 2018). The data are derived from laboratory measurements of whole air samples collected by Programmable Flask Package (PFP) onboard the two ACT-America aircraft (Baier et al., 2020). The two aircraft conducted five six-week field campaigns spanning the Central and Eastern US (27°S-49°N, 106°W-73°W) covering all four seasons from 2016 through 2019, including late summer 2016 (July–August), winter 2017 (February–March), fall 2017 (October–November), spring 2018 (April–May), and early summer 2019 (June–July). Each campaign focused on sampling three unique regions, which are defined here as Northeast (NE: 35-45°N, 85-75°W), Midwest (MW: 37-45°N, 100-87°W), and South (~28-37°N, 100-85°W). These regions (and corresponding flask samples) are shown in Figure 1, and color coded as blue, red, and green for the remainder of the paper.

Approximately 10–12 flask samples were captured during each flight. We screen data for overlapping high quality samples of CO_2, CO, and COS and fair-weather days (~50% of total samples, ranging from 32% in
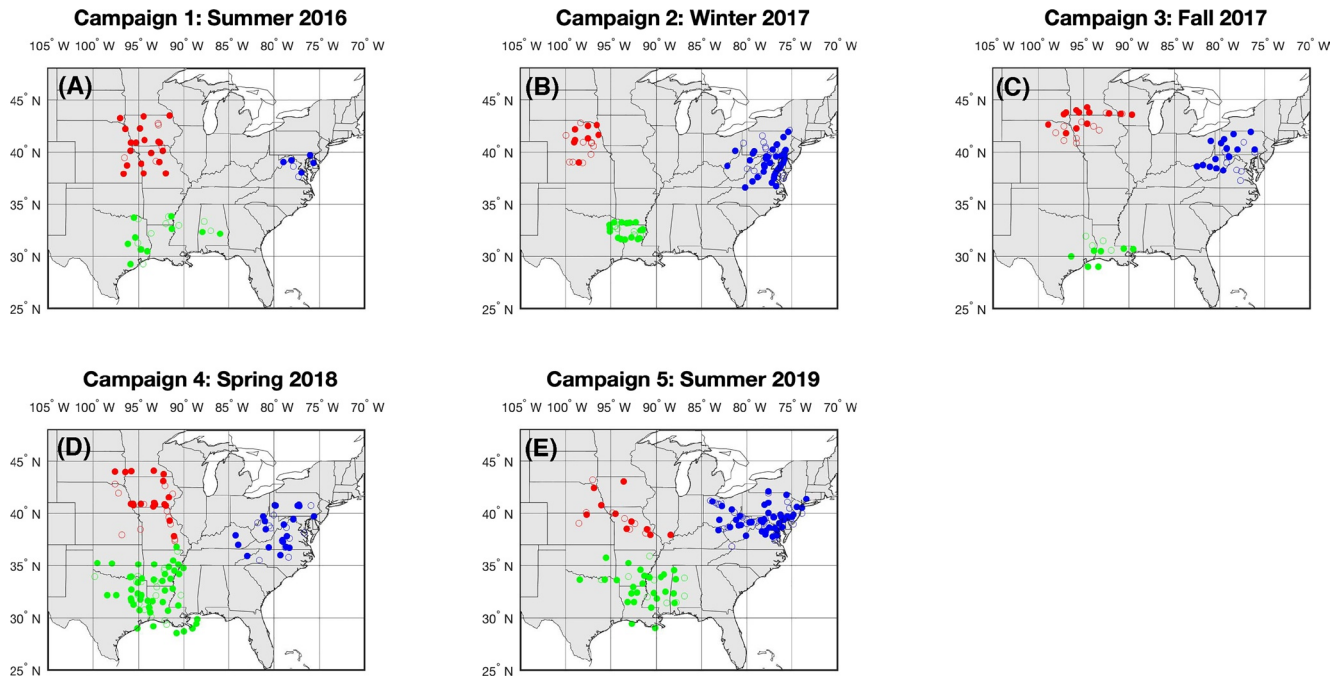
Figure 1. Total remaining Portable Flask Package samples per campaign after screening for fair weather days and overlapping high quality CO_2, COS, and CO data. Samples are color coded by region (Red = Midwest, Green = South, Blue = Northeast). Filled circles denote boundary layer samples (altitude <2 km agl).

fall 2017 to 59% in summer 2019) using provided air mass flags (Wei et al., 2021). CO_2 samples collected during summer 2016 were replaced by continuous data from *in situ* systems on board both aircraft due to CO_2 depletion in undried flask air samples at water vapor levels above 1.7% (Baier et al., 2020). Water vapor dependencies on COS (e.g., COS hydrolysis) in undried flasks were evaluated in all 2016 ACT flasks and further, more extensive testing was conducted through laboratory studies within dried and undried PFPs. Neither tests have shown significant indication of COS hydrolysis effects in the ACT glass flasks to-date. Thus, we expect any COS hydrolysis effects to be within the uncertainty of the ACT COS measurements (stated in Baier et al., 2020). However, nearly half of COS measurements analyzed during the first campaign failed to pass quality control criteria due to air sample contamination of COS measurements from o-rings, leading to reduced sample size in summer 2016 (52 flask samples) compared to subsequent campaigns (58–133). The total number of remaining samples per campaign ranges from 52 to 105 in the first three campaigns, and increases to 127 and 133 in the final two campaigns, respectively. In particular, we note a nearly factor of three increase in sample size from summer 2016 to summer 2019.

Aircraft tracks were designed to be within (~300 m AGL) or above the boundary layer (BL) as observed by on-board thermodynamics and lidar data. We focus on enhancements of tracer concentrations within BL relative to background variability in order to maximize sensitivity to local-regional (~100–500 km) surface flux influences. We estimate BL enhancements as the difference between BL and free troposphere (FT) flask data as indicated by metadata flags (Wei et al., 2021). Baier et al. (2020) show that FT data provides an effective measure of background conditions for CO_2 in winter. We provide additional simulation experiments using global atmospheric tracer simulations further justifying the use of FT data to define background conditions for all tracers and seasons studied here (Text S1). We denote BL enhancements (BL – FT) as ΔCO_2, ΔCO, and ΔCOS.

To estimate enhancements, we further sort data into BL and FT bins using provided flags, with BL data denoted by filled circles in Figure 1. The nature of this aircraft campaign is such that BL and FT data were not always collected in the same location. Rather, data were collected along level-altitude transects that were hundreds of kilometers long, and encompassed synoptic weather patterns, causing spatial disconnect between BL and FT samples. We therefore average all FT data collected in a single day to represent a mean background value per day. Specifically, for each day with at least one flask sample in the BL and FT, we take
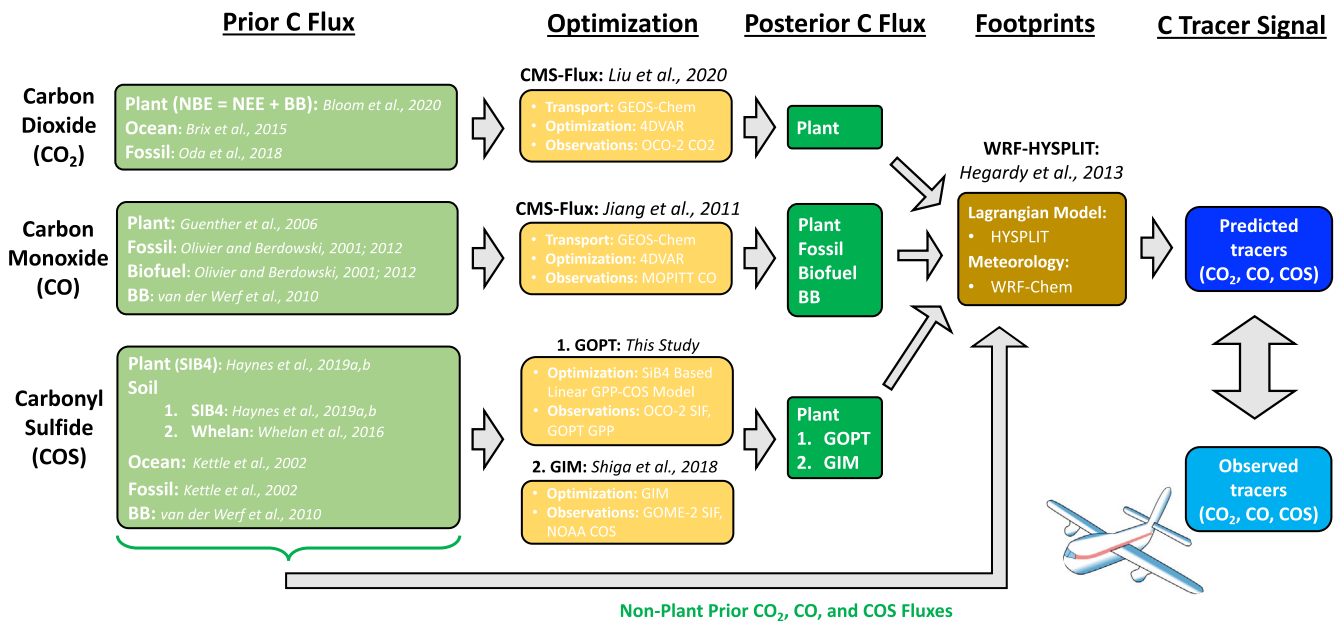
Figure 2. Schematic of model analysis in this study, focused on prediction of atmospheric tracer concentrations (CO_2, CO, and COS) and comparison to Atmospheric Carbon Transport-America airborne data. Prior estimates of tracer surface flux, representing biogenic, oceanic, and anthropogenic processes, are prescribed for each tracer (light green shading). Plant based biogenic fluxes (for CO_2, CO and COS) and non-biogenic fluxes (CO) are constrained against satellite and in situ observations of CO_2 (OCO-2), CO (MOPITT), and COS (NOAA, OCO-2 SIF), and using various optimization techniques (light brown). Optimized posterior fluxes (dark green) are combined with non-biogenic prior fluxes, convolved with surface influence functions (footprints) derived from Lagrangian modeling (dark brown) to predict atmospheric tracer concentrations (dark blue) at the sampling time and location of airborne flask samples (light blue), and analyzed against each other.

the mean value of all FT data, and subtract that from individual BL samples. By limiting the flight data to fair-weather conditions, we minimize large horizontal gradients associated for example with frontal boundaries (e.g., Baier et al., 2020), increase the likelihood that the BL and FT data represent the same air mass, minimize the potential for cloud convection to spread surface flux signatures into the FT, and reduce cloudy light limiting periods, thus optimizing conditions for photosynthesis and biogenic signals.

2.2. Posterior Tracer Surface Fluxes

In order to interpret the observed atmospheric tracer distributions, model atmospheric simulations are forced by surface fluxes of CO_2, COS, and CO. In this study, we aim to use a set of surface fluxes that are consistent with various observational data-streams. These surface fluxes are derived from a combination of "top-down" (i.e., posterior fluxes constrained by atmospheric data) and "bottom-up" (i.e., prior fluxes derived from land-surface models or ancillary data). For CO_2 and CO, we start with climatological "bottom-up" prior fluxes, and derive posterior fluxes using OCO-2 (for CO_2) and Measurements of Pollution in the Troposphere (MOPITT) (for CO). For COS, we explore three independent process-based and data-constrained estimates of plant COS uptake. The data and methods used to calculate these fluxes are summarized below. The prediction of tracer signals from surface fluxes are summarized in Section 2.3. A flow chart of our analysis is provided in Figure 2.

2.2.1. CO_2 Flux

Net CO_2 flux is composed of the sum of net biosphere exchange (NBE, representing the sum of net ecosystem exchange (NEE) + biomass burning), air-sea net CO_2 exchanges (Ocean), and fossil fuel emissions. The net carbon balance and its constituent fluxes are derived from the Carbon Monitoring System Flux (CMS-Flux) system (http://cmsflux.jpl.nasa.gov). The net or "total" flux is constrained over the period 2015–2019 against column integrated CO_2 from OCO-2 using a 4D-Var inversion system, based on the adjoint of the GEOS-Chem global transport model at $4° \times 5°$ degree spatial resolution (Liu et al., 2014; Liu, Baskaran, et al., 2020 and references therein). Over land, the posterior net carbon flux from CMS-Flux is attributed
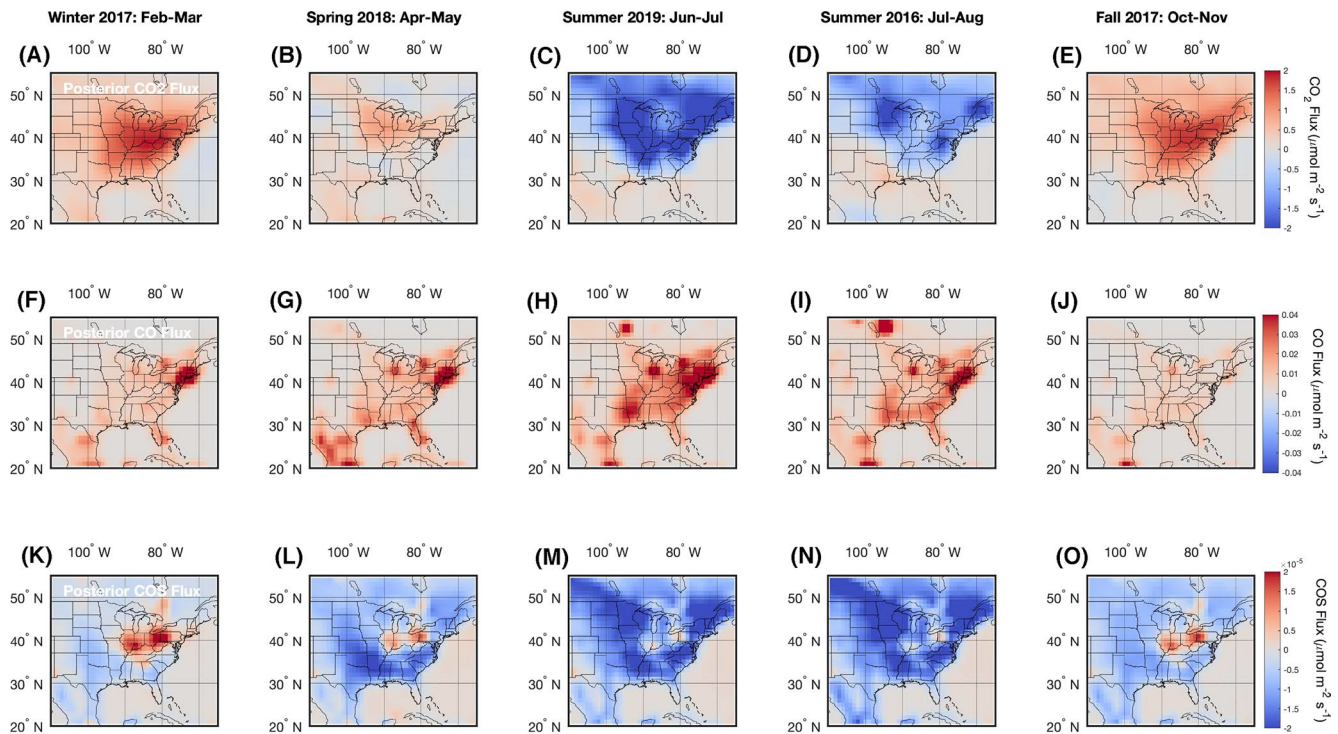
Figure 3. Posterior surface fluxes of CO_2, CO, and COS corresponding to the five Atmospheric Carbon Transport-America campaigns from 2016 to 2019. Flux maps are time-resolved (1–3 hr) but plotted here as the two-month average over each campaign period in order of season and month(s) of year. Posterior fluxes are constrained by satellite observations using global top-down inversion methods for CO_2 and CO, and bottom-up geostatistical inversion methods for COS (GIM). Prior fluxes from which posterior fluxes are derived are not shown, but exhibit similar spatial patterns which are scaled up or down using inverse methods. Surface fluxes of COS derived using the SIB4 model and OCO-2 SIF constraints (GOPT) are not shown. Time resolved fluxes are then convolved with 10-day HYSPLIT footprints for each flask sample, which are shown in Figure 5.

to NBE as it is the largest source of variability in atmospheric CO_2. The resulting posterior NBE adjusts the prior or "bottom-up" NBE estimates from the CARDAMOM model-data fusion system, summarized in Bloom et al. (2016, 2020), which itself is constrained by multiple data streams including GOME-2 SIF, MODIS Leaf Area Index, above-ground biomass, and soil carbon for NEE, and FLUXCOM GPP and Global Fire Emissions Database version 4 (GFEDv4) for biomass burning.

Additional prior fluxes in CMS-Flux include ocean and fossil emissions summarized in Brix et al. (2015), Carroll et al. (2020), and Oda et al. (2018). In order to link these fluxes to aircraft measurements, prior and posterior monthly fluxes are downscaled to 3-h timescales for diurnal footprint analysis of ACT-America samples (Section 2.3) using ERA-interim reanalysis of global radiation and surface temperature, following the approach of Olsen and Randerson (2004).

2.2.2. CO Flux

Posterior CO fluxes in CMS-Flux are derived using a similar 4D-Var approach as is used for CO_2 (Jiang et al., 2015; Kopacz et al., 2009, 2010), using CO observations from MOPITT instrument. This approach is summarized in more detail in Bowman et al. (2017) and Worden et al. (2019). Following Jiang et al. (2011), each month is estimated independently with initial conditions supplied by a suboptimal Kalman filter (Parrington et al., 2008). The configuration for the CO inversion follows Jiang et al. (2013) where the control vector for CO emissions combines the combustion, biogenic, and methane CO sources. We note that, while the inversion conserves mass globally and across the annual cycle, this often leads to imbalances in time, space, and flux components in the posterior solution. For example, the inversion fails to preserve strong year-round fossil emissions in the Northeast in the prior (discussed below), including increased emissions in winter (e.g., Figure 3). Instead, we find increased emissions in summer, and reduced emissions in winter.

Prior CO flux components used in the inversion include combustion CO sources (fossil fuel, biofuel, and biomass burning), and CO oxidation from biogenic non-methane VOCs and methane. Atmospheric CO oxidation is assumed to occur within the relatively coarse 4 × 5 scales, such that CO surface emissions occur in the same grid box as precursor emissions. Biomass burning emissions are obtained from GFED4 (van der Werf et al., 2010). Anthropogenic emissions (fossil fuel and biofuel) combine off-line emission inventories from the Emission Database for Global Atmospheric Research global model (EDGAR v4.2; Olivier & Berdowski, 2001) and regional models over North America (Kuhns et al., 2003) propagating seasonal, weekly, and diurnal variation. We do not account for net soil uptake of CO, which we acknowledge could partially offset combustion and biogenic sources in the southeast US (e.g., Liu et al., 2018). Biogenic and biomass emissions are estimated at 3-hourly resolution, other fluxes are monthly.

Precursor emissions of CO from biogenic sources are computed using the Model of Emissions of Gases and Aerosols from Nature (MEGAN) version 2.0 (Guenther et al., 2006). MEGAN models the VOC emission with three parameters, an annual emission factor, an activity factor, and a production and loss rate. The emission factor represents the emission of a compound at standard condition where the activity factor represents the emission changes due to deviations from standard condition. Emissions are calculated for each plant functional type and summed to estimate the total emission per grid cell accounting for regional variations in vegetation type, leaf area index, canopy maturity, solar angle, surface temperature, and soil moisture (Guenther et al., 2006). Biogenic CO emissions combine 30% isoprene, 20% monoterpene, and 67% acetone emission. The regional distribution in North America is characterized by isoprene dominance in the southeast US (Figure S3).

2.2.3. COS Flux

We examine three independent process-based and data-constrained estimates of plant COS uptake from (a) the Simple Biosphere Model version 4 (SiB4) process model, (b) atmospheric data-constrained and independent geostatistical inverse modeling (GIM) framework, and (c) semi-empirical SIF-based constraint (GOPT). These products are described in more detail below. We note that SiB4 and GIM estimates are not year specific, and thus do not represent climate conditions at the time of ACT-America data collection. Other COS component fluxes prescribed in this study include soil uptake (Whelan et al., 2016), anthropogenic emissions (Kettle et al., 2002), biomass burning (van der Werf et al., 2010), and oceanic emissions (Kettle et al., 2002). The same component fluxes are prescribed for each estimate of plant COS uptake, with the exception that SiB4 uses its own soil uptake, as described below.

2.2.3.1. SiB4

The Simple Biosphere Model (SiB4; Haynes, Baker, Denning, Stöckli, et al., 2019, Haynes, Baker, Denning, Wolf, et al., 2019) is a mechanistic and process-based model that simulates land-atmosphere exchanges of energy, momentum and moisture, as well as the terrestrial carbon cycle. By simulating biogeochemical and biophysical processes over heterogeneous vegetation, SiB4 not only provides estimates of water, energy and carbon fluxes, but it also predicts a wide variety of land characteristics and properties, including soil moisture, soil carbon pools, biomass, leaf area index, albedo, COS, and SIF. To create a self-consistent, predictive model, SiB4 combines elements from a prognostic phenology model (SiBpp; Stöckli et al., 2008, 2011), a crop model (SiBcrop; Corbin et al., 2010; Lokupitiya et al., 2009), and a terrestrial carbon pool model (SiB-CASA; Schaefer et al., 2008, 2009) into a single modeling framework. By combining the processes from these three previous versions of SiB and using tiles of plant functional types (PFTs) to represent land cover heterogeneity, SiB4 can investigate land surface properties and land-atmospheric exchanges on a variety of temporal and spatial scales.

Plant uptake of atmospheric CO_2 and COS are directly related to photosynthesis through diffusion by stomatal conductance and consumption by collocated reaction in the chloroplasts of leaves (Rubisco and carbonic anhydrase (CA), respectively) (Berry et al., 2013; Campbell et al., 2008). Diffusion of gases including CO_2, COS, and water vapor along the pathway from the atmosphere to leaf cell where biochemistry takes place is controlled by boundary layer, stomatal, and mesophyll conductance (Berry et al., 2013). The prognostic canopy air space in SiB4, and addition of mesophyll conductance scaling to Vcmax (and modulation by environmental conditions), enables direct calculations of plant COS uptake (Baker et al., 2003; Stöckli & Vidale, 2005).

SiB4 has its own representation of soil COS exchange, which accounts for biotic uptake and respiration. In more productive environments, CA accumulates in the surface litter and near-surface soil, and thus respire more COS and as function of productivity (Berry et al., 2013). Estimates of soil uptake from Whelan et al. (2016) are derived from an empirical model based on temperature and moisture, which accounts for biotic uptake and abiotic exchange. Both soil flux estimates show net uptake on average, but differ significantly in magnitude and spatial pattern in the eastern US (Figure S4). Despite clear differences in spatial variability, soil exchange is small relative to plant uptake, and has negligible impact on atmospheric signal predictions (e.g., Figure S5) or tracer-tracer regressions.

2.2.3.2. GIM

Atmospheric trace gas applications of the GIM framework have primarily been used to estimate surface net ecosystem exchange CO_2 fluxes (Michalak, 2004) by coupling atmospheric trace gas observations to a model of atmospheric transport. The GIM framework allows for the incorporation of covariate datasets to help constrain the space-time patterns of surface flux estimates (Gourdji et al., 2008, 2012). The GIM approach used here optimizes plant COS fluxes over North America using COS observations from the NOAA airborne network (https://www.esrl.noaa.gov/gmd/ccgg/aircraft/) and remotely sensed SIF (GOME-2, Joiner et al., 2013) as a single covariate. SIF is used as a covariate to help the inversion capture the space time patterns of photosynthetic CO_2 and hence plant COS fluxes. This approach is based on a North American regional CO_2 inversion (Shiga et al., 2018) using the same pre-computed footprint library created from the WRF-STILT atmospheric transport model (Nehrkorn et al., 2010) runs for NOAA's CarbonTracker Lagrange project (https://www.esrl.noaa.gov/gmd/ccgg/carbontracker-lagrange/). The influence of the background is removed by subtracting the average of observations above 2.5 km in any given aircraft sampling profile from the observations in the lowest 1.5 km (boundary layer).

The inversion also accounts for the influence from secondary COS fluxes from soils (Whelan et al., 2016), anthropogenic emissions (Zumkehr et al., 2018), and biomass burning (Stinecipher et al., 2019). We acknowledge uncertainty of GIM COS to secondary fluxes, especially with respect to soil COS fluxes given large differences in magnitude and spatial variability of available estimates in the eastern US (Figure S4). Overall, soil COS uptake from Whelan et al. (2016) is larger than that of SiB4, leading to less plant COS uptake in our inversion, but providing the best match to available NOAA COS data.

To isolate plant COS fluxes, the influence from secondary COS fluxes have been removed by convolving these surface fluxes with the WRF-STILT footprints and then subtracting from the boundary layer observations. Plant COS fluxes are optimized yearly at 1×1 spatial resolution over North America from 2008 to 2012 using four different sets of covariance parameters assuming two different model-data mismatch variances and two different temporal correlation lengths (see Table S1). A 5-year climatology of the monthly average of these four inversion runs is used here to reduce the impact of both data gaps and the impact of covariance parameter choices.

2.2.3.3. GOPT

As mentioned above, plant uptake of atmospheric COS is directly related to photosynthesis through diffusion modulated by stomatal conductance. Even though most terrestrial biosphere models include a representation of stomatal conductance enabling prediction of GPP, and multiple empirical-based methods exist for constraining GPP against satellite vegetation data (Anav et al., 2015), most models don't simulate leaf COS uptake. To get around this limitation, we developed a simplified biome-specified linear regression method that converts GPP into COS plant uptake from the mechanism in the SIB4 model, effectively accounting for changes in leaf relative uptake (LRU) between PFTs. Analysis of monthly mean plant COS and GPP output from SiB4 shows a biome-dependent linear relationship. Therefore, we compute the linear regressions from GPP to COS flux for broad MODIS-based biome classifications. We compute the regression between GPP and COS plant uptake data for each biome (ib) from SIB4 output in the following form:

$$\text{COS}_{ib}(x, y) = k_{ib}\,\text{GPP}(x, y) + b_{ib} \tag{1}$$

where x and y are latitude and longitude coordinates. By applying the consistent biome specified regression model, we can derive COS plant uptake from any GPP product. A limitation of this simplified model is time-invariant assumption in LRU leading to potential divergent nighttime pathways of COS (uptake)
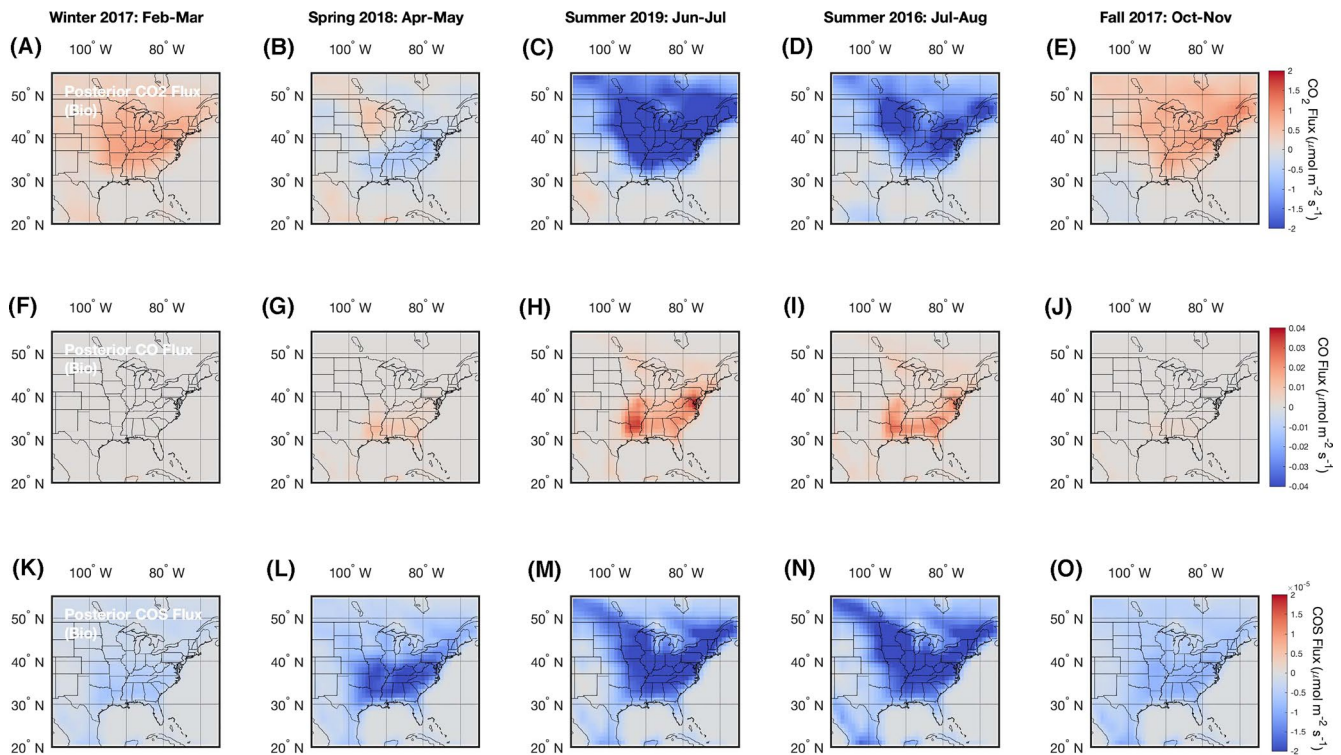
Figure 4. Same as Figure 3, but for plant component of total flux.

versus CO_2 (respiration). Here, we derived SIF-based GPP estimates following Parazoo et al. (2014), where year-specific monthly GPP at each grid point is inferred from a precision-weight minimization of spaceborne SIF, which is regressed against global GPP from upscaled flux tower data (e.g., Frankenberg et al., 2011; Jung et al., 2011) and subjected to prior knowledge of GPP from an ensemble of terrestrial ecosystem models (Sitch et al., 2015). This method is updated here using OCO-2 measured SIF constraints. Monthly GPP is downscaled to 3 h using the same approach for NBE, and then used in Equation 1 to estimate COS.

2.2.3.4. Total Versus Biogenic Flux

Seasonal maps of posterior CO_2, CO, (from CMS-Flux) and COS flux (from GIM) are shown in Figure 3. The corresponding biogenic component is shown in Figure 4. For CO_2 and COS, total and biogenic fluxes show consistent magnitude and spatial distribution over the entire year. The main difference can be seen in the northeast and upper Midwest, where fossil fuel emissions are prevalent. Fossil emissions drive most of the COS flux and amplify CO_2 emissions in winter, and offset much of the plant-driven COS drawdown in summer. The CO posterior is driven largely by hotspots of emissions from fossil fuel (year-round) and fires in summer. Biogenic emissions occur mainly in summer in the south, lower Midwest, and along the mid-Atlantic regions, and show consistent magnitude from early to late summer (June–August).

2.3. Atmospheric Signal Prediction

The preceding posterior fluxes are derived from atmospheric models run at fairly coarse spatial resolution. As such, when these fluxes are propagated back to the atmosphere using the same atmospheric models run in forward simulation mode, they will not capture the variability seen in the ACT-America samples. To bridge those scales, we run the HYbrid Single-Particle Lagrangian Integrated Trajectory (HYSPLIT) model (Draxler & Hess, 1997; Stein et al., 2015) in Stochastic Time-Inverted Lagrangian Transport (STILT)-emulation mode and driven by meteorological fields from the Weather Research and Forecasting Chemistry model (WRF-Chem; Feng, Lauvaux, Klaus, et al., 2019) to estimates surface influence (footprint) predictions for ACT-America flask samples. WRF-HYSPLIT shows comparable skill to WRF-STILT in simulating tracer plumes and surface footprints when driven by the same meteorology (Hegarty et al., 2013).
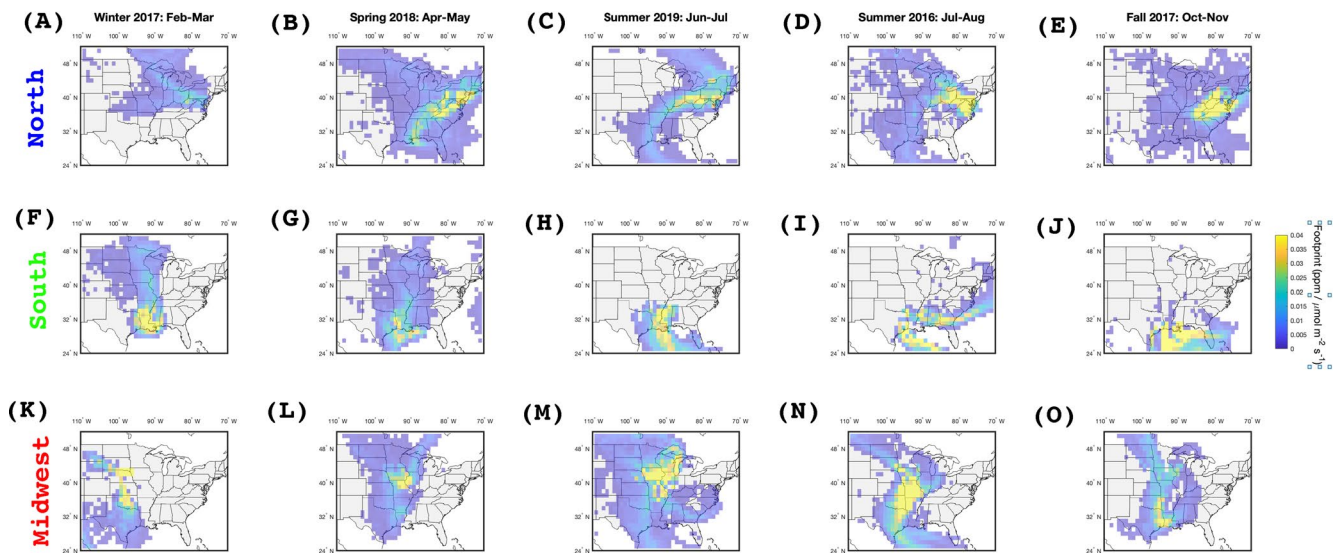
Figure 5. Concentration footprints corresponding to boundary layer flask data collected during five Atmospheric Carbon Transport campaigns. Footprints are organized by campaign (columns, in order of season and month(s) of year) and flask sampling region (Northeast in top row; South in middle row; Midwest in bottom row). Footprints are derived for each flask sample using surface influence functions from the HYSPLIT langrangian back trajectory model, and convolved with time resolved prior and posterior fluxes to determine predicted signals for comparison with observed signals. Footprints shown here represent a data-collection time average, with footprints from individual samples summed over the previous 10 days, and then averaged across all samples within each region for each campaign.

The WRF-Chem simulation is carried out using version 3.6.1. The domain of interest contains most of North America [170°W - 60°W, 20°N - 75°N] at 27 km horizontal resolution. The model has 50 levels up to 50 hPa with 20 levels in the lowest 1 km. The model meteorology is initialized every 5 days and driven with ERA5 reanalysis every 6 h at 25-km horizontal resolution. The WRF-Chem dynamic is relaxed to ERA5 (Hersbach et al., 2020) meteorology every 6 h using grid nudging. Each meteorological re-initialization is started at a 12-h setback from the end of the previous 5-day run. The first 12 hours of every 5-day simulation are considered spin-up and discarded from the final analysis. We also update sea surface temperature every 6 h at 12-km resolution. Choices of the model physics parameterizations used in this experiment are documented as the baseline setup described in Feng, Lauvaux, Klaus, et al. (2019) and Feng, Lauvaux,Williams, et al. (2019). Specifically, MYNN 2.5 PBL scheme (Nakanishi & Niino, 2004) and Noah Land surface model (Feng, Lauvaux,Williams, et al., 2019) are used for vertical mixing.

WRF-HYSPLIT was run backward for 10 days, or until particles exit the North American continental boundary, roughly defined by the WRF-Chem domain above. For each back trajectory, 500 particles were released at each flask receptor location to generate footprints every 15 min along the particle trajectories. Surface footprints were re-calculated on a 1-degree grid and saved at hourly intervals. Surface influences for each region and campaign are shown in Figure 5.

We note several differences in summer influence patterns in 2016 and 2019. The NE region shows more local influence in 2016, and westerly and northerly influence in 2019. The MW region has a larger southerly component in 2016. The S region is more southerly and easterly in 2016, and has more local and southerly influence in 2019. We also note a strong influence from the Gulf of Mexico in both years.

3. Results

We refer to prior and posterior surface fluxes in Figures 3 and 4 as F_{CO_2}, F_{CO}, and F_{COS}, with positive values indicating a net source (or emission) of tracer from land to the atmosphere, and negative values indicating a net sink (or uptake) of tracer from atmosphere to land. Observed seasonal tracer distribution in the BL and FT, and corresponding enhancements (Δ = BL - FT), are shown in Figure S6 (top and bottom rows, respectively). Comparison to predicted enhancements, determined by convolving prior and posterior surface fluxes with HYSPLIT influence functions, is provided in Figure 6. We refer to $\Delta < 0$ (BL < FT) as depletion
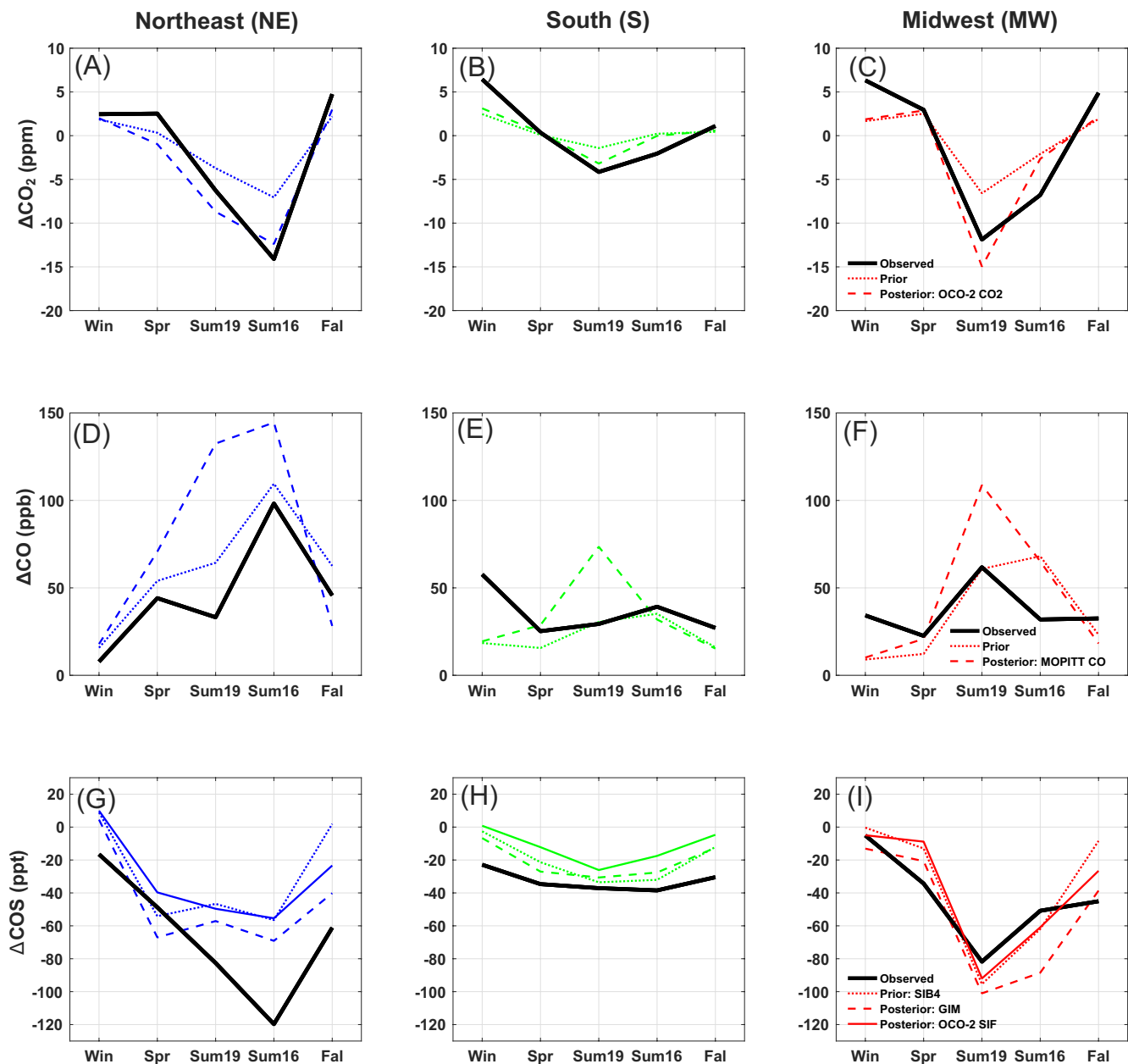
Figure 6. Observed and satellite constrained (prior and posterior) seasonal tracer enhancement (Δ = FT – BL), separated by region (columns). Observed enhancements as in Figure S3. Satellite constrained fluxes are convolved with WRF-STILT footprints to determine atmospheric concentrations at Atmospheric Carbon Transport flask samples. Prior fluxes are derived from a range of natural and anthropogenic model and inventory estimates (see main text). Posterior CO_2 fluxes (top row) are constrained by OCO-2 CO_2. COS fluxes are derived from SiB4, the GIM geostatistical inversion, and OCO-2 SIF linear regression model. Posterior CO derived from MOPITT CO.

and $\Delta > 0$ (BL > FT) as enrichment. We also refer to CO production by biogenic VOCs as "biogenic CO emission."

3.1. Observed Tracer Seasonal Enhancements

We point out several important features regarding seasonal amplitude and timing of observed tracer variations, and seasonal covariance across tracers. In particular, ΔCO_2 drawdown is consistently deeper and earlier in the BL compared to the FT across our three study regions, leading to net depletion in early and late summer, and net enrichment in fall, winter, and spring (Figure S6). Focusing on BL enhancements, we note

that the magnitude of peak ΔCO_2 depletion roughly follows the north-south gradient, with deeper depletion in the NE and MW (Figures 6a and 6c) and shallowest depletion in the S (Figure 5b). The timing of peak depletion occurs in late summer in the NE, and early summer in MW and S. The seasonal and regional patterns are expected, but still encouraging given the inconsistent sampling of these regions in space and time.

ΔCOS shows positive seasonal correlation with ΔCO_2 in each region ($r^2 = [0.48, 0.90]$; see Table S2), including similar seasonal timing and magnitude. ΔCOS remains depleted on average in fall when ΔCO_2 becomes enriched, but the summer-to-fall tendency (reduced depletion) is in the same direction. Interestingly, peak ΔCO enhancement occurs in early and late summer in MW and NE, respectively, corresponding to peak ΔCOS and ΔCO_2 depletion, producing seasonal anti-correlation between ΔCOS-ΔCO and ΔCO_2-ΔCO in the MW and NE. Winter ΔCO enrichment in the MW and S is synchronized with peak ΔCO_2 enrichment, and negligible ΔCOS depletion, consistent with the dominance of a fossil fuel source.

3.2. Comparison of Observed and Simulated Seasonal Enhancements

Predicted signals from prior and posterior fluxes show surprisingly good agreement with observations in terms of seasonal timing, magnitude, and relative variability across tracers and regions (Figure 6 and Table S3). In most cases, predicted and observed tracer-tracer correlations have the same sign, including positive correlation of ΔCO_2-ΔCOS in all three regions, and negative correlation of ΔCO_2-ΔCO and ΔCOS-ΔCO in the NE and S regions. Similar seasonal and tracer-correlation patterns are found for prior and posterior flux estimates, with the following caveats: (a) significantly improved agreement in seasonal magnitude in ΔCO_2 posteriors (mean regression slope per region increases from 0.43 to 0.74; Table S3), (b) degraded seasonal amplitude but improved structure in the ΔCO posterior, and (c) seasonally coherent but regionally dependent performance in COS flux estimates. With these considerations, we can use the observationally constrained model simulations to interpret seasonal and spatially variable biospheric influences on observed enhancement patterns, through comparison of posterior flux and surface influence maps (Figures 3–5) as discussed below.

We focus first on summer ΔCO_2 depletion in the NE region (Figure 6a). The predominant surface influences occur within the Appalachian deciduous broadleaf forests (~40°N, 80°W), where posterior F_{COS} and F_{CO2} show regionally strong sinks, and F_{CO} shows a locally strong source. COS and CO_2 biogenic sinks are only slightly offset by anthropogenic emissions, while the CO source is persistent year-round but amplified by summer biogenic sources. The difference in timing of peak surface F_{CO2} uptake (early summer 2019) and peak ΔCO_2 depletion (late summer 2016) points to other important influences besides the seasonal change in surface flux magnitude. In this case, we note a shift in the location and magnitude of the surface influence function, from a locally strong NE influence in late summer 2016, centered near a local sink hotspot in West Virginia, to a weaker westerly influence in early summer 2019. The shift in upstream influence is most likely driven by differences in predominant weather patterns on the sampling days and locations in 2016 versus 2019; other possible factors are discussed in more detail in Section 4.

Observed summer depletion of ΔCO_2 and ΔCOS in the MW region (Figures 6c and 6i) is driven by strong F_{COS} and F_{CO2} uptake across the Central Great Plains and into southern Canada. Enhanced depletion in summer 2019 is consistent with stronger influence over crop dominated landscapes in the upper Midwest. Reduced depletion of ΔCO_2 and ΔCOS occurs on days with stronger southerly influence (from −13 ppm to −5 ppm for ΔCO_2 and −80 ppt to −67 ppt for ΔCOS, on average). By contrast, these same days show a relative increase in ΔCO enrichment, aligned with a biogenic F_{CO} source along the Mississippi River in southern Arkansas (Figures 4h and 4i). Likewise, reduced ΔCO_2 and ΔCOS depletion in summer 2016 (relative to summer 2019) is linked to a pattern of predominantly southerly influence in 15 of 19 flask samples. Days with more northerly influence show increased depletion of ΔCO_2 and ΔCOS (from −6 ppm to −11 ppm for ΔCO_2 and −39 ppt to −53 ppt for ΔCOS), and decreased ΔCO enrichment (from 18 to 17 ppb). These results suggest a strong influence of crops and northern ecosystems on biogenic drawdown of CO_2 and COS in the MW, a weak influence of crops on CO (slight decrease in ΔCO enrichment), and potential biogenic surface source of CO along the southern portion of the Mississippi River (which is overestimated in posterior estimates).

Flask data collected in the S region show a much stronger offshore surface and background influence compared to other regions. The reduced terrestrial influence compared to MW and NE regions partially explains the relatively weak magnitude of summer ΔCO_2 depletion (Figure 6b). It's worth noting, however, increased ΔCOS depletion and ΔCO enrichment in summer 2016 (in the S), corresponding to increased influence from the southeast US where biogenic F_{CO} emissions and F_{COS} uptake are prevalent (but potentially underestimated in our prior and posterior models). We also find a strong local influence along the Mississippi river in summer 2019 where posterior F_{CO} emissions peak. This surface posterior F_{CO} source appears to have the same biogenic origin as southerly influenced MW flask samples, and is most likely responsible for the predicted ΔCO enrichment spike in summer 2019, which is nevertheless overestimated compared to observations.

Observed ΔCO_2 enrichment in the NE region in winter (Figure 6a) is consistent with fossil emissions and annually persistent F_{CO} emissions (Zumkehr et al., 2018). Observed and simulated ΔCO_2 show diverging patterns in spring, with excessive depletion in predicted signals, indicative of excessive prior and posterior biogenic uptake. We find similar patterns in the S and MW regions, with less local fossil F_{CO} and F_{COS} influence (near Chicago) in spring.

3.3. Tracer-Tracer Spatial Correlations Across Individual BL Flasks

The analysis in Section 3.2 focused on seasonally averaged tracers and their covariations, providing an informative assessment of regionally and seasonally integrated fluxes. We are also interested in how the spatial distribution of fluxes affects the correlation between individual flask samples. For this, we examine the spatial covariance between tracers across individual flasks per region and season, for observed and predicted enhancements. The results are plotted as seasonal regression slopes in Figure 7, with values that are significantly different from zero and well correlated ($R^2 > 0.25$) denoted by symbols. An example regression for a single season and region is shown in Figures 8a and 8b. The number of BL samples per region ranges from 8 (S region, summer 2016) to 78 (NE region, summer 2019).

From an observational perspective, most regions and seasons show no significant spatial covariation. However, we note several important covariations that facilitate our interpretation of seasonal tracer depletion and enrichment. In particular, the S region shows persistent and significant negative correlation between ΔCO_2-ΔCO and ΔCOS-ΔCO, and positive correlation between ΔCO_2-ΔCOS, from early summer through late fall (Figures 6b, 6h, and 6e, respectively). We observe similar tracer-tracer patterns in late summer in the MW region, and the positive relationship between ΔCO_2 and ΔCOS in summer is consistent with tower-based measurements of F_{CO2} and F_{COS} flux at a maize field in Illinois (Figure S7). These patterns are consistent with land-based biological depletion of ΔCO_2 (plant-driven ΔCOS and ΔCO_2 depletion increases with ΔCO enrichment), but only lead to net regional ΔCO_2 depletion from early to late summer with surface influences over the southern US (more discussion below). These tracer-tracer patterns continue into fall, but are inconsistent with ΔCO_2 enrichment, and occur as surface influences shift offshore, making inferences of a persistent southern biogenic F_{CO2} sink into fall inconclusive.

Predicted enhancements from prior and posterior fluxes capture the negative ΔCOS-ΔCO correlation in summer 2019, and increased regression slope in summer 2016, but underestimate the slope of regression by a factor of 2 (Figure 7h; -1.67 ± 0.29 vs. -0.852 ± 0.14). Predicted signals also underestimate the slope of ΔCO_2-ΔCOS regression by a factor of 3 (Figure 7e; 0.0675 ± 0.026 vs. 0.0265 ± 0.018). The results suggest that models underestimate southern growing season CO_2 uptake, and ΔCO_2 depletion, due to weak photosynthetic drawdown upstream of flask samples.

We can investigate the effect of flux spatial variability on late summer ΔCOS-ΔCO correlation, and subsequent model bias, in more detail through closer examination of individual flask samples. Only three total days of campaign data were collected in summer 2016, with two days (August 27-28) influenced primarily by the southeast US (easterly influence swath in Figure 5i), with high ΔCO and low ΔCOS air, and the other day (August 24) under more local to southerly influence from Gulf inflow, with high ΔCOS and low ΔCO air (Figure 8a). It follows that the observed ΔCOS-ΔCO negative correlation is driven in large part by covariance of F_{CO} precursor emissions and F_{COS} uptake in the southeast US. As such, increasing the biogenic component of posterior F_{CO2} (NBE) and F_{COS} (plant) uptake by factors of 2 each in the southeast region,
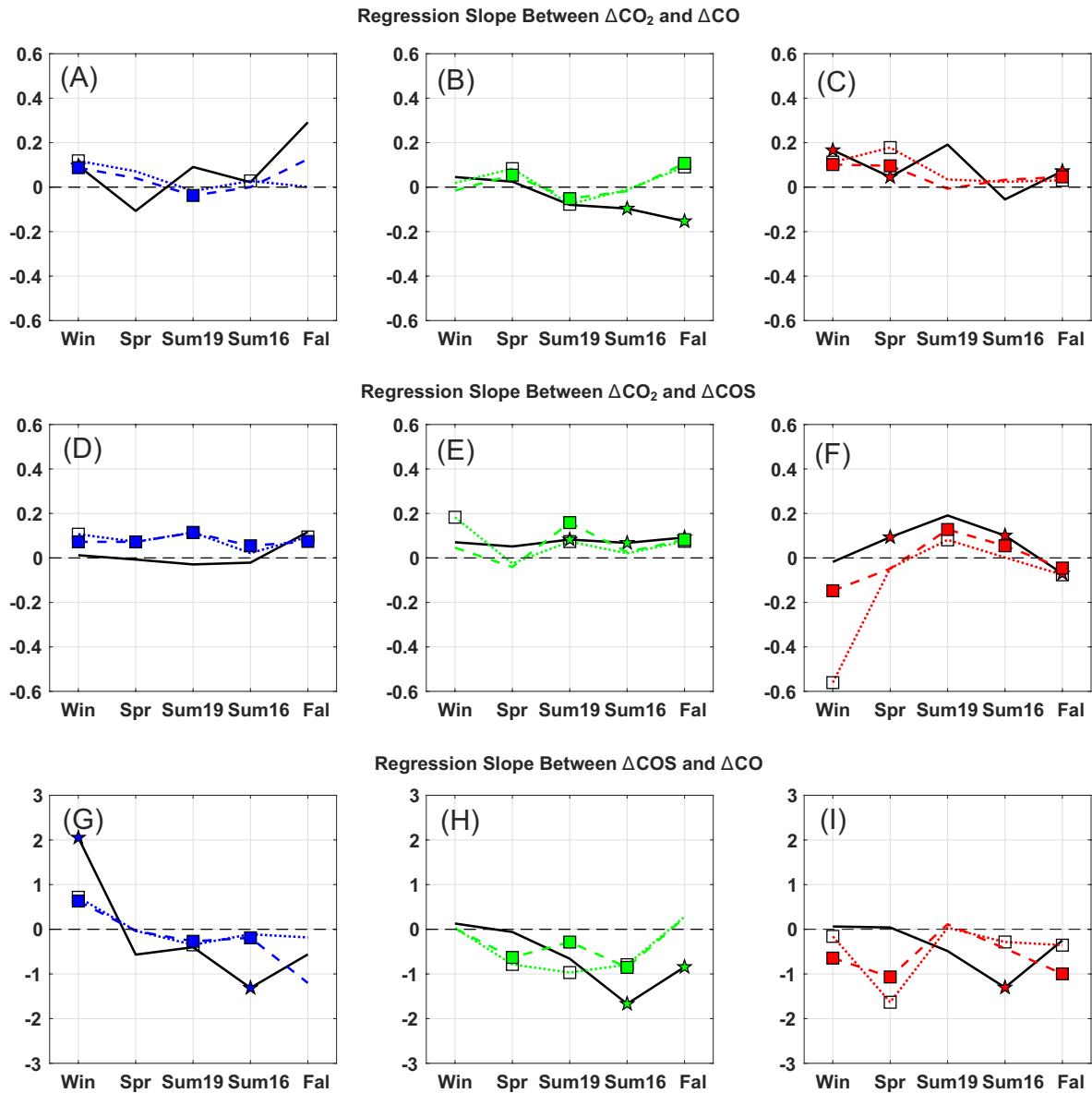
Figure 7. Multi-tracer spatial regression. Each point represents the slope of the spatial regression between tracer enhancements across all boundary layer samples within a single season and region, including ΔCO_2 and ΔCO (top row), ΔCO_2 and ΔCOS (middle row), and ΔCOS and ΔCO (bottom row). Observed regressions are shown in black, simulated regressions in color, and regions are color coded. Markers represent points with statistically significant regressions (slope significantly different from zero, $r^2 > 0.25$). Simulated regressions are based on prior (dotted) and posterior (dashed fluxes). Only results for SIB4 (dotted) and GIM (dashed) are shown for ΔCOS regressions.

defined here as 90-80°W, 28-36°N, substantially improves the agreement between predicted and observed tracer-tracer correlation patterns in the South region (Figures 8b–8d), as well as absolute values of ΔCO_2 depletion (from −0.025 ppm to −0.85 ppm, Figure 6b). Regression slopes in the South increase by ~50% for ΔCOS-ΔCO (from −0.852 to −1.48 ppt/ppb), ~30% for ΔCO_2-ΔCOS (from +0.0265 to +0.033 ppm/ppt), and ~300% for ΔCO_2-ΔCO (from −0.018 to −0.05 ppm/ppb). For ΔCO_2-ΔCOS, we note that increasing the posterior biogenic F_{COS} alone actually degrades the correlation, and that the combination of F_{COS} and F_{CO_2} is needed (Figure 8h). The need for increased F_{COS} and F_{CO_2} uptake, and no change in F_{CO}, is consistent with seasonal comparisons (Figure 7), which show that posteriors underestimate observed ΔCO_2 and ΔCOS depletions at regional scale in late summer 2016.
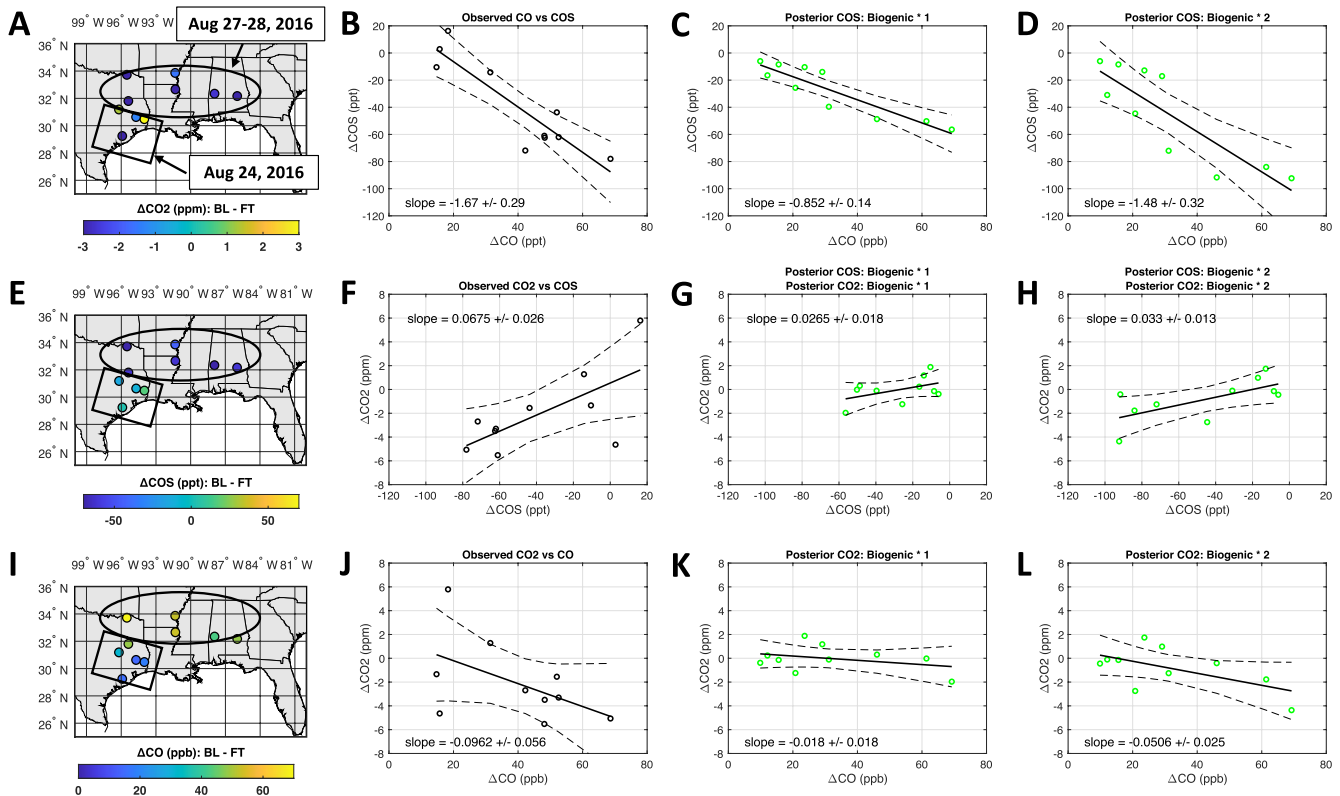
Figure 8. Surface flux drivers of observed tracer-tracer correlations in Atmospheric Carbon Transport-America South region in Summer 2016. (a, e, i) Observed ΔCO and ΔCOS mole fractions show distinct spatial gradients, with lower ΔCO/higher ΔCOS to the southwest (August 24, 2016) and higher ΔCO/lower ΔCOS to the northeast (August 27–28, 2016). Observed and simulated tracer-tracer regression slopes for ΔCOS-ΔCO (b-d), $ΔCO_2$-ΔCOS (f-h), and $ΔCO_2$-ΔCO (j-l). (b, f, j) Observed regressions, (c, g, k) Posterior regressions, (d, h, l) Posterior regressions based on perturbed fluxes of ΔCOS and $ΔCO_2$, determined by multiplying biogenic flux components within the southern region (90°W-80°W, 28°N-36°N) by a factor of 2 (denoted by * in title).

The trajectories from the south also have a big impact on the MW region, and to a lesser extent the NE region (Figure 5). As such, sensitivity runs impact simulated tracer-tracer slopes in other regions. For example, doubling biogenic COS and CO_2 uptake increases the slope of ΔCOS-ΔCO in the Midwest by 50% (−0.428 to −0.658 ppt/ppb). Decreasing Biogenic CO emissions by half increases ΔCOS-ΔCO slope in the MW by another 11%, and reduces the high summer ΔCO enrichment bias in the MW.

Perturbation experiments with biogenic CO and oceanic COS demonstrate additional flux sensitivities. First, while a change in biogenic CO flux is not necessary in our current setup (which does not account for the offsetting effect of soil CO uptake) decreasing the biospheric F_{CO} emission by a factor of 2 further increases the predicted ΔCOS-ΔCO slope by 20% (to −1.78 ppt/ppb) in much closer agreement with the observed slope (Figure S8). This demonstrates the important correlation of biogenic F_{COS} and F_{CO}, and strong influence of isoprene emissions in the south (Figure S3). By contrast, reducing F_{CO} fossil emissions by half increases the ΔCOS-ΔCO slope by 2%.

Finally, increasing indirect emissions of oceanic COS from carbon disulfide (CS_2) by a factor of 10 increases the ΔCOS-ΔCO slope by 8% (from −1.48 to −1.55 ppt/ppb) in closer agreement with observations. This is surprising because similar increases in significantly stronger oceanic sources (direct COS and indirect COS from dimethyl sulfide, or DMS; Figure S9) have negligible impact on ΔCOS-ΔCO. Further examination of spatial variability of perturbed ocean emissions in the Gulf of Mexico reveal unique spatial patterns for each oceanic component (Figure S10), including a more prominent north-south and east-west gradient for indirect COS by CS_2. While acknowledging the challenge in properly simulating atmospheric circulations along the sea/land interface especially for coarse models, this result highlights that it is just as important to properly characterize COS magnitude, spatial pattern, and source over ocean as it is over the land. This

is particularly true for the interpretation of BL enhancements of COS in regions such as the southern US which experience strong inflow from ocean.

The ΔCOS-ΔCO correlation is further improved by considering salt marsh emissions as an additional process not typically encountered in regional COS budgets. Salt marsh ecosystems are large emitters of COS. Instantaneous saline wetland emissions range from ~0 to 300 pmol m^{-2} s^{-1} (). A surface flux campaign along the Texas shore of the Gulf of Mexico, within the footprint of August 24 ACT-America data analyzed here, estimated an average flux from vegetated plots of ~60 pmol m^{-2} s^{-1}, with larger emissions in July sometimes exceeding 110 pmol m^{-2} s^{-1} (Whelan et al., 2013). To assess the sensitivity of predicted ΔCOS-ΔCO correlations in the S region to salt marshes, we add salt marsh emissions to our total posterior COS flux by assuming a mean value of 70 pmol m^{-2} s^{-1} in July within gulf coast pixels and that vegetated salt marshes comprise ~200 km^2 of the Texas Gulf Coast in 2016 (extrapolating from Armitage et al., 2015). We note that the objective here is not to capture salt marshes exactly, but rather to provide a realistic estimate to demonstrate sensitivity of airborne tracer-tracer correlation patterns. Including salt marsh F_{COS} emissions increases the spatial gradient of total F_{COS}, which acts on the spatial gradient of atmospheric signals in a small but non-trivial way, and increases the slope of regression of ΔCOS-ΔCO by 5%, from −1.48 to −1.55 (not shown).

4. Discussion

We analyzed boundary layer enhancements (BL – FT) of biologically sensitive tracer species (CO_2, COS, CO) collected by ACT-America aircraft campaigns over four seasons and five campaigns from 2016 to 2019 against a corresponding set of independent, satellite-constrained surface fluxes to determine the spatial and seasonal influence of plant uptake on atmospheric CO_2 enhancements. We find a strong gradient of ΔCO_2 and ΔCOS drawdown from north to south, peaking in the northeast US in late summer, consistent with wider geographic region of influence in northern regions (eastern US + Canada) and limited upwind influence area in the S region. Our main result indicates a common terrestrial biogenic sink of CO_2 and COS and biogenic source of CO in summer spread mostly evenly throughout the eastern US, driven by uptake of CO_2 and COS by vegetation, and emission of biogenic VOCs, through stomatal conductance. In general, the magnitude, timing, and regional dependence of the summer CO_2 sink is well estimated by a CMS-Flux inversion system constrained by OCO-2 observed column CO_2, and represents a significant improvement over model-based estimates (based on increase in mean seasonal regression with observed values from 0.43 to 0.73).

We provide evidence that the magnitude of the terrestrial CO_2 sink, however, is underestimated by prior and satellite constrained models in the temperate humid forests in the southeast US. In particular, strong depletion of ΔCO_2 and ΔCOS and enrichment of ΔCO is observed in flask data from August 27–28, 2016 in the southern US. The resulting significant negative regression between ΔCOS and ΔCO is underestimated by predicted signals, and requires a factor of 2 or more larger biogenic uptake than is estimated by CO_2 and COS inversion models, and potentially less emissions of biogenic CO (Figures 6b, 6e, 6h).

Our main results are broadly consistent with findings from a similar study led by Hilton et al. (2017), who benchmarked land surface estimates of F_{COS} uptake against airborne COS profiles, and found models with strong crop driven GPP uptake in the Midwest to be the most consistent with observations. However, we argue that this finding must be reframed in the context of unprecedented sampling of the southern US offered by ACT-America, and in particular the meteorological conditions during the two days from August 27–28, 2016 with surface influences originating in the southeast US, which otherwise have negligible influence on the findings here or in Hilton et al. (2017). As such, regionally focused ACT-America flights suggest that GPP activity is driving summer CO_2 sinks throughout the eastern US, with the strongest sinks in the Midwest and Northeast regions, and stronger than expected sinks in the Southeast.

Our results suggest that models capture first order processes (temperature, sunlight) driving regional stomatal conductance and seasonal photosynthetic exchange of carbon in the south, and thus predicted and observed tracer-tracer regressions have the same sign. However, the observed tracer-tracer relationships are much stronger than expected, especially in summer 2016. While acknowledging the uncertainty that our small flask sample size contributes to observed relationships, we also recognize several missing processes

and errors in model representation that may contribute to the weak predicted relationship. We have already explored several plausible scenarios for COS, including unaccounted for COS emissions from coastal salt marsh and CS_2 and DMS production in the Gulf of Mexico. We offer several additional hypotheses to explain low terrestrial CO_2 uptake.

Our primary hypothesis is that model GPP is too weak in the south, as indicated in parallel studies of ACT-America data (Cui et al., 2021; Feng et al., 2021), and plant CO_2/COS uptake sensitivity experiments in this study. Parallel studies of the CASA biosphere model attribute low uptake to missing agricultural sinks from management that leads to biomass removal in late summer (Feng et al., 2021). Indeed, this process drives net uptake of CO_2 from a top-down perspective, and explains the high bias in CO_2 depletion seen in South and Midwest regions in Summer 2016 (e.g., Figure 6). We see examples of this in flux tower observations obtained from Delta Flux (Runkle et al., 2017), for example due to rice cultivation in Arkansas (e.g., Figure S11 and Table S4). However, harvest doesn't explain our low GPP bias, since removing crops would reduce GPP and stomatal conductance, and weaken the observed ΔCOS-ΔCO relationships. Alternatively, there are cases of strong agricultural CO_2 uptake through late summer driven by ample water and sun, for example by sugarcane in Louisiana (Figure S11), which are unlikely to be represented by CASA, or the underlying CARDAMOM model of CMS-Flux presented here. Managed urban and sub-urban environments are also likely to increase the fraction of carbon uptake in summer, especially under dry conditions (e.g., Miller et al., 2020). In general, we acknowledge that gradients and diversity of managed and unmanaged landscapes across the Mississippi Delta, representing a key region of influence in this study, present a formidable challenge for biosphere models and atmospheric inversions. While future studies should look more carefully into the influence of agriculture on atmospheric concentrations in the South, it doesn't appear to have a significant influence on the results presented here.

An alternative hypothesis for low summer GPP, mainly specific to this study, is the lack of C4 grass representation in CARDAMOM. We note the strong presence of C4 plants within the footprint of southern flask samples, including the Arkansas-Louisiana region (see Figure S12), which were not included in the version of the underlying CARDAMOM model of CMS-Flux. As such, our CO_2 flux results do not account for increased heat tolerance of C4 plants in summer 2016, which would drive increased GPP on days with stronger influence from regions west of the Mississippi Delta. Further examination of C4 versus C3 influences on CO_2 and COS under heat stressed conditions should also account for lower LRU values in C4 plants (e.g., Stimler et al., 2011), which will diminish the influence on COS.

This also highlights a potential limitation in using spaceborne SIF to constrain GPP and COS together. While our SIF constrained COS models (GIM and OCO-2 SIF) and NEE models (CARDAMOM) capture the basic structure of the annual cycle, they do not capture the depth of growing season COS depletion in the Northeast and Southern regions with as much fidelity as in the Midwest. SIF provides a well-known indicator for GPP in crop regions which are typically irrigated and not subject to water stress, and can continue to photosynthesis in high light/high temperature conditions conducive to both increased SIF and stomatal conductance. As such, one possible implication is that SIF does not provide as accurate a measure of COS and/or GPP in the late growing season in temperate evergreen and deciduous forests in the South and Northeast, respectively, due to increased dissipation of light through other pathways such as sustained nonphotochemical quenching (e.g., Raczka et al., 2019). Additionally, photosynthetic uptake by understory vegetation is largely unobserved by satellites, contributing to low biases in SIF and GPP.

Our secondary hypothesis is that models underestimate net CO_2 uptake in the South due to considerable disequilibrium (GPP/Respiration >1) of southeastern temperate forests, due in part the assumption of constant in time carbon use efficiency (Bradford & Crowther, 2013). Such a mechanism would lead to long term carbon storage and higher than expected depletion of ΔCOS and ΔCO_2 on days with strong influence from regions east of the Mississippi Delta (Figures 5 and 8). This hypothesis is better supported by our flux sensitivity experiments requiring doubling of southern plant uptake of COS and CO_2 to better match observed tracer-tracer relationships. Possible mechanisms include a stronger than expected CO_2 fertilization effect on GPP and biomass accumulation, and land use change associated with forest aggradation, consistent for example with increased wood pellet production in the southeast US (Wang et al., 2015). This hypothesis is plausible and highly intriguing, but highly uncertain given the limited available data with sensitivity to the Southeast.

The unexpected strong negative relationship between ΔCOS and ΔCO suggests that (a) tracers such as COS and CO_2 can provide important independent constraints of modeled biogenic CO emissions and (b) biogenic CO has potential for diagnosing interannual- to decadal- scale change in biogenic processes. While biogenic CO is not directly related to GPP variability, our results suggest there are strong linkages between biogeochemistry and productivity that could provide mechanistic insight over larger scales. However, current MOPITT constrained CO emissions are limited by the spatially coarse native resolution (2° × 2.5°) of our inversion and unaccounted for processes such as soil CO uptake (e.g., Liu et al., 2018), causing a mixture of sectors and processes, and confounding biogenic emissions with combustion sources and soil sinks. Additionally, CO variability is substantial near the surface and in the free troposphere, which can cause misattribution of local versus distance sources. It is also challenging to link CO to precursor emissions without also leveraging information from measurements sensitive to precursor emissions, such as isoprene and monoterpene. While beyond the scope of this study, one could in principle combine CO, isoprene, and monoterpene data from aircraft and satellites into a full chemical adjoint for more refined estimates of biogenic CO and precursor emissions. In addition, ingestion of higher spatial resolution CO data from TRO-POMI (Martínez-Alonso et al., 2020) and CrIS (Buchholz et al., 2021; Fu et al., 2016) with multiconstituent chemical data assimilation techniques (Miyazaki et al., 2020) could substantially improve the attribution of CO variability to sectoral and natural emissions.

All three regions show observed net depletion of ΔCOS and enrichment of ΔCO_2 and ΔCO in Fall 2017, significantly so in the Northeast, which points to a GPP sink of COS and CO_2 in the fall but of insufficient magnitude to offset soil respiration and fossil fuel emissions (Baier et al., 2020). Moreover, all models underestimate fall ΔCOS depletion, and underestimate ΔCO_2 and ΔCO enrichment. While underestimated plant GPP uptake is a likely model culprit in the summer, it is unlikely to explain the divergent patterns of ΔCOS and ΔCO_2 in fall, the latter of which would require larger compensating low biases in respiration and/or fossil emissions. We do note, however, systematic model underestimates of ΔCO_2 enrichment in winter and spring, when soils and plants are less active, suggesting that F_{CO2} respiration sources are underestimated. This points to the possibility of fossil emissions as the additional fall F_{CO2} source, and soils as a missing fall COS sink.

While seasonal tracer behavior follows expected patterns from seasonally variable biogenic sources, it also reflects year to year variability in weather, upstream surface influence, and climate. Our findings are based on the reconstructed seasonal cycle derived from five 6-week snapshots (winter, spring, early summer, late summer, and fall) over a period of four years. We caution the reader about over-interpretation of our seasonal cycle as climatologically persistent features. Interannual variability in climate drivers, ecosystem response, emissions change, flask sampling frequency and location, atmospheric winds, background variability, and upstream surface influences can have strong impacts on observed variability within a given year, season, and weather system. For example, we note a factor of 3 fewer samples in the Northeast region in summer 2016 versus summer 2019, different surface influence regions between each campaign, extreme flooding in Louisiana in summer 2016 followed by a drought pattern in the south in 2016, which likely increased water limitation in plants in late summer, and extreme flooding in the Midwest in summer 2019 which delaying planting of crops (Yin et al., 2020). We also note that our background calculation, derived from limited data in the free troposphere, is subject to uncertainty especially in cases when BL and FT air do not share the same air mass. Except for the two days from August 27–28, 2016, the South region is influenced almost entirely by offshore background flow from the Gulf of Mexico. While unlikely, it is possible that conditions exist for which ΔCO_2 depletion is stronger in the South than in the Northeast, for example under a stably stratified atmosphere and more direct influence from the southeast US. While continuous observations of COS are a challenge, there exists a wealth of continuous *in situ* CO_2 data from ACT-America and surface towers in the Southeast (in Alabama and Mississippi) over the same period as the flask samples analyzed here (Miles et al., 2018). We recommend future efforts leveraging these data for more targeted study of surface influences from this critical region than is possible from our airborne based flask analysis.

Finally, while our predicted signals show high fidelity in capturing observed patterns of variability, we note several key model limitations. Satellite CO_2 and CO inversions are constrained by column integrated observations, which are subject to spatially coherent and poorly constrained biases, and strongly dependent on transport models, which are subject to horizontal and vertical transport uncertainty (Parazoo et al., 2012;

Schuh et al., 2019) especially along the land-sea interface of the Gulf Coast. OCO-2 observations are relatively sparse along the southern coast (e.g., Figure S13), which further limits constraints on the southern land sink and Gulf inflow. Including ocean glint observations could improve posterior flux estimates. Posterior fluxes are spatially coarse, ranging from $2° \times 2.5°$ in the CO inversion model and $4° \times 5°$ in CO_2 inversion model, making it difficult to separate anthropogenic emissions from biogenic fluxes in dense urban regions such as the Northeast, or separate land from ocean along the Gulf Coast. Future efforts should examine CT2019 North America $1° \times 1°$ posterior fluxes for more detailed assessment of seasonal CO_2 uptake in the South region or nested regional CO_2 inversions at 0.5 degrees or better. We also note that top-down inversion estimates are derived as monthly means, and then temporally downscaled to daily resolution using solar radiation, and thus do not capture the true day-to-day variability as seen in the flask data. Additionally, our SIF-based estimates (GOPT) assume a linear relationship between SIF and GPP, and furthermore derive the relationship to COS using a linear model derived from SiB4 output. These estimates provide a realistic first guess, but more sophisticated SIF models accounting for non-photochemical quenching (e.g., Magney et al., 2020; Parazoo et al., 2020) are needed for accurate predictions of COS and GPP from observed SIF.

5. Conclusions

ACT-America airborne campaigns acquired vertically resolved observations of biologically sensitive carbon species including CO_2, COS, and CO in flask samples, providing unprecedented insight into the seasonal and spatial distribution of carbon sinks across diverse bioclimatic regions in the eastern US. Our model-observation tracer-tracer analysis of boundary layer flask enhancements supports previous findings that biogenic CO_2 drawdown, and subsequent timing and magnitude of ΔCO_2 depletion, is spatially variable across the eastern US. Crops in the upper Midwest drive strong ΔCO_2 and ΔCOS depletion from early to late summer. Temperate forest in the Northeast drive strong ΔCO_2 and ΔCOS depletion in late summer. The unprecedented ACT-America flask samples uncovered evidence that humid temperate forests in the poorly constrained South continue to photosynthesize and absorb CO_2 and COS (and emit CO through biogenic VOC precursor emissions) deeper into the growing season than expected by model priors and posteriors. However, additional sampling in the South is needed to conclusively constrain the carbon dynamics of this under-sampled region. Predicted atmospheric signals based on satellite constrained inversion fluxes (CMS-Flux) reproduce much of the observed seasonal and regional variability, as well as variability across tracers, and indicate a stronger than expected sink of CO_2 in humid temperate forests in the southeast. Ongoing analysis of ACT-America data with respect to independent satellite-constrained fluxes is needed to understand the impact of confounding sources of variability in temporally sparse airborne acquisitions (e.g., interannual variability in climate, transport, surface influence, and background flow), and refine missing carbon source and sink processes.

Data Availability Statement

ACT-America flask observations for all 5 airborne campaigns from 2016 to 2019 are archived at ORNL (https://doi.org/10.3334/ORNLDAAC/1593). Prior and posterior surface fluxes for CO_2 (NBE) are available at https://cmsflux.jpl.nasa.gov/get-data/nbe-2020. COS fluxes derived using the GIM model are available as monthly average values from 2008 to 2012 at https://zenodo.org/record/4304602#.X8kSj6pKjIE. HY-SPLIT footprints used in the calculation of predicted atmospheric tracer signals are currently available at ftp://aftp.cmdl.noaa.gov/pub/baier/, but will move to ftp://aftp.cmdl.noaa.gov/products/carbontracker/lagrange/footprints/ACT/ during the review process. COS fluxes from SiB4 are available at https://daac.ornl.gov/CMS/guides/SiB4_Global_HalfDegree_Monthly.html. Assimilated atmospheric COS concentrations from the COS-OCS model (see Supporting Information S1) are available through Ma et al. (2021). Prior and posterior CO emissions, and COS derived from the GOPT method, will be made available at https://cmsflux.jpl.nasa.gov/.

References

Anav, A., Friedlingstein, P., Beer, C., Ciais, P., Harper, A., Jones, C., et al. (2015). Spatiotemporal patterns of terrestrial gross primary production: A review. *Reviews of Geophysics*, *53*(3), 785–818. https://doi.org/10.1002/2015RG000483

Armitage, A. R., Highfield, W. E., Brody, S. D., & Louchouarn, P. (2015). The contribution of mangrove expansion to salt marsh loss on the Texas Gulf Coast. *PloS One*, *10*(5), e0125404. https://doi.org/10.1371/journal.pone.0125404

Arneth, A., Sitch, S., Pongratz, J., Stocker, B. D., Ciais, P., Poulter, B., et al. (2017). Historical carbon dioxide emissions caused by land-use changes are possibly larger than assumed. *Nature Geoscience*, *10*(2), 79–84. https://doi.org/10.1038/ngeo2882

Baier, B. C., Sweeney, C., Choi, Y., Davis, K. J., DiGangi, J. P., Feng, S., et al. (2020). Multispecies assessment of factors influencing regional CO_2 and CH_4 enhancements during the winter 2017 ACT-America campaign. *Journal of Geophysical Research: Atmospheres*, *125*, e2019JD031339. https://doi.org/10.1029/2019JD031339

Baker, I., Denning, A. S., Hanan, N., Prihodko, L., Uliasz, M., Vidale, P. L., et al. (2003). Simulated and observed fluxes of sensible and latent heat and CO_2 at the WLEF-TV tower using SiB2.5. *Global Change Biology*, *9*(9), 1262–1277. https://doi.org/10.1046/j.1365-2486.2003.00671.x

Berry, J., Wolf, A., Campbell, J. E., Baker, I., Blake, N., Blake, D., et al. (2013). A coupled model of the global cycles of carbonyl sulfide and CO_2: A possible new window on the carbon cycle. *Journal of Geophysical Research: Biogeosciences*, *118*(2), 842–852. https://doi.org/10.1002/jgrg.20068

Bloom, A. A., Bowman, K. W., Liu, J., Konings, A. G., Worden, J. R., Parazoo, N. C., et al. (2020). Lagged effects dominate the inter-annual variability of the 2010-2015 tropical carbon balance. *Biogeosciences*, *17*, 6393–6422. https://doi.org/10.5194/bg-2019-459

Bloom, A. A., Exbrayat, J.-F., van der Velde, I. R., Feng, L., & Williams, M. (2016). The decadal state of the terrestrial carbon cycle: Global retrievals of terrestrial carbon allocation, pools, and residence times. *Proceedings of the National Academy of Sciences of the United States of America*, *113*(5), 1285–1290. https://doi.org/10.1073/pnas.1515160113

Bowman, K. W., Liu, J., Bloom, A. A., Parazoo, N. C., Lee, M., Jiang, Z., et al. (2017). Global and Brazilian carbon response to El Niño Modoki 2011–2010. *Earth and Space Science*, *4*(10), 637–660. https://doi.org/10.1002/2016EA000204

Bradford, M. A., & Crowther, T. W. (2013). Carbon use efficiency and storage in terrestrial ecosystems. *New Phytologist*, *199*(1), 7–9. https://doi.org/10.1111/nph.12334

Brix, H., Menemenlis, D., Hill, C., Dutkiewicz, S., Jahn, O., Wang, D., et al. (2015). Using Green's Functions to initialize and adjust a global, eddying ocean biogeochemistry general circulation model. *Ocean Modelling*, *95*, 1–14. https://doi.org/10.1016/j.ocemod.2015.07.008

Buchholz, R. R., Worden, H. M., Park, M., Francis, G., Deeter, M. N., Edwards, D. P., et al. (2021). Air pollution trends measured from Terra: CO and AOD over industrial, fire-prone, and background regions. *Remote Sensing of Environment*, *256*, 112275. https://doi.org/10.1016/j.rse.2020.112275

Byrne, B., Liu, J., Bloom, A. A., Bowman, K. W., Butterfield, Z., Joiner, J., et al. (2020). Contrasting regional carbon cycle responses to seasonal climate anomalies across the east-west divide of temperate North America. *Global Biogeochemical Cycles*, *34*(11), e2020GB006598. https://doi.org/10.1029/2020gb006598

Byrne, B., Liu, J., Lee, M., Baker, I., Bowman, K. W., Deutscher, N. M., et al. (2020). Improved constraints on northern extratropical CO_2 fluxes obtained by combining surface-based and space-based atmospheric CO_2 measurements. *Journal of Geophysical Research: Atmospheres*, *125*(15), e2019JD032029. https://doi.org/10.1029/2019JD032029

Campbell, J. E., Carmichael, G. R., Chai, T., Mena-Carrasco, M., Tang, Y., Blake, D. R., et al. (2008). Photosynthetic control of atmospheric carbonyl sulfide during the growing season. *Science*, *322*(5904), 1085–1088. https://doi.org/10.1126/science.1164015

Carroll, D., Menemenlis, D., Adkins, J. F., Bowman, K. W., Brix, H., Dutkiewicz, S., et al. (2020). The ECCO-Darwin data-assimilative global ocean biogeochemistry model: Estimates of seasonal to multidecadal surface ocean pCO_2 and air-sea CO_2 flux. *Journal of Advances in Modeling Earth Systems*, *12*(10), e2019MS001888. https://doi.org/10.1029/2019ms001888

Corbin, K. D., Denning, A. S., Lokupitiya, E. Y., Schuh, A. E., Davis, K. J., Miles, N., et al. (2010). Assessing the impact of crops on regional CO_2 fluxes and atmospheric concentrations. *Tellus*, *62*, 521–532. https://doi.org/10.1111/j.1600-0889.2010.00485.x

Cui, Y. Y., Jacobson, A. R., Feng, S., Wesloh, D., Barkley, Z. R., Zhang, L., et al. (2021). Evaluation of CarbonTracker's inverse estimates of North American net ecosystem exchange of CO_2 from different observing systems using ACT-America airborne observations. *Journal of Geophysical Research: Atmospheres*, *126*(12), e2020JD034406. https://doi.org/10.1029/2020jd034406

Davis, K. J., Browell, E. V., Feng, S., Lauvaux, T., Obland, M. D., Pal, S., et al. (2021). The Atmospheric Carbon and Transport (ACT)–America Mission. *Bulletin of the American Meteorological Society*, 1–54. https://doi.org/10.1175/bams-d-20-0300.1

Davis, K. J., Obland, M. D., Lin, B., Lauvaux, T., O'Dell, C., Meadows, B., et al. (2018). *ACT-America: L3 merged in situ atmospheric trace gases and flask data, eastern USA*. Oak Ridge, Tennessee, USA: ORNL DAAC. https://doi.org/10.3334/ORNLDAAC/1593

Draxler, R. R., & Hess, G. D. (1997). *Description of the HYSPLIT4 modeling system*.

Feng, S., Lauvaux, T., Davis, K., Keller, K., Zhou, Y., Willimans, C., et al. (2019). Seasonal characteristics of model uncertainties from biogenic fluxes, transport, and large-scale boundary inflow in atmospheric CO_2 simulations over North America. *Journal of Geophysical Research: Atmospheres*, *124*, 14325–14346. https://doi.org/10.1029/2019JD031165

Feng, S., Lauvaux, T., Klaus, K., Davis, K., Rayner, P., Oda, T., & Gurney, K. (2019). A road map for improving the treatment of uncertainties in high-resolution regional carbon flux estimates. *Geophysical Research Letters*, *46*, 13461–13469. https://doi.org/10.1029/2019GL082987

Feng, S., Lauvaux, T., Williams, C. A., Davis, K. J., Zhou, Y., Baker, I., et al. (2021). Joint CO_2 mole fraction and flux analysis confirms missing processes in CASA terrestrial carbon uptake over North America. *Global Biogeochemical Cycles*, *35*, e2020GB006914. https://doi.org/10.1029/2020GB006914

Frankenberg, C., Fisher, J. B., Worden, J., Badgley, G., Saatchi, S. S., Lee, J., & Kuze, A. (2011). New global observations of the terrestrial carbon cycle from GOSAT: Patterns of plant fluorescence with gross primary productivity. *Geophysical Research Letters*, *38*(17), L17706. https://doi.org/10.1029/2011gl048738

Fu, D., Bowman, K. W., Worden, H. M., Natraj, V., Worden, J. R., Yu, S., et al. (2016). High-resolution tropospheric carbon monoxide profiles retrieved from CrIS and TROPOMI. *Atmospheric Measurement Techniques*, *9*(6), 2567–2579. https://doi.org/10.5194/amt-9-2567-2016

Gourdji, S. M., Mueller, K. L., Schaefer, K., & Michalak, A. M. (2008). Global monthly averaged CO_2 fluxes recovered using a geostatistical inverse modeling approach: 2. Results including auxiliary environmental data. *Journal of Geophysical Research*, *113*(D21), D21115. https://doi.org/10.1029/2007jd009733

Gourdji, S. M., Mueller, K. L., Yadav, V., Huntzinger, D. N., Andrews, A. E., Trudeau, M., et al. (2012). North American CO_2 exchange: Inter-comparison of modeled estimates with results from a fine-scale atmospheric inversion. *Biogeosciences*, *9*(1), 457–475. https://doi.org/10.5194/bg-9-457-2012

Guanter, L., Zhang, Y., Jung, M., Joiner, J., Voigt, M., Berry, J. A., et al. (2014). Global and time-resolved monitoring of crop photosynthesis with chlorophyll fluorescence. *Proceedings of the National Academy of Sciences of the United States of America*, *111*(14), E1327–E1333. https://doi.org/10.1073/pnas.1320008111

Guenther, A., Karl, T., Harley, P., Wiedinmyer, C., Palmer, P. I., & Geron, C. (2006). Estimates of global terrestrial isoprene emissions using MEGAN (Model of Emissions of Gases and Aerosols from Nature). *Atmospheric Chemistry and Physics*, *6*, 3181–3210. https://doi.org/10.5194/acp-6-3181-2006

Haynes, K. D., Baker, I. T., Denning, A. S., Stöckli, R., Schaefer, K., Lokupitiya, E. Y., & Haynes, J. M. (2019). Representing ecosystems using dynamic prognostic phenology based on biological growth stages: Part 1. Implementation in the Simple Biosphere Model (SiB4). (Accepted for Publication) *Journal of Advances in Modeling Earth Systems*, *11*, 4423–4439. https://doi.org/10.1029/2018MS001540

Haynes, K. D., Baker, I. T., Denning, A. S., Wolf, S., Wohlfahrt, G., Kiely, G., & Minaya, R. C. (2019). Representing ecosystems using dynamic prognostic phenology based on biological growth stages: Part 2. Grassland carbon cycling. (Accepted for Publication) *Journal of Advances in Modeling Earth Systems*, *11*, 4440–4465. https://doi.org/10.1029/2018MS001541

Hegarty, J., Draxler, R. R., Stein, A. F., Brioude, J., Mountain, M., Eluszkiewicz, J., et al. (2013). Evaluation of Lagrangian particle dispersion models with measurements from controlled tracer releases. *Journal of Applied Meteorology and Climatology*, *52*(12), 2623–2637. https://doi.org/10.1175/jamc-d-13-0125.1

Hersbach, H., Bell, B., Berrisford, P., Hirahara, S., Horányi, A., Muñoz-Sabater, J., et al. (2020). The ERA5 global reanalysis. *Quarterly Journal of the Royal Meteorological Society*, *146*(730), 1999–2049. https://doi.org/10.1002/qj.3803

Hilton, T. W. (2018). Photosynthesis in high definition. *Nature Climate Change*, *8*(1), 20–21. https://doi.org/10.1038/s41558-017-0040-6

Hilton, T. W., Whelan, M. E., Zumkehr, A., Kulkarni, S., Berry, J. A., Baker, I. T., et al. (2017). Peak growing season gross uptake of carbon in North America is largest in the Midwest USA. *Nature Climate Change*, *7*(6), 450–454. https://doi.org/10.1038/nclimate3272

Hudman, R. C., Murray, L. T., Jacob, D. J., Millet, D. B., Turquety, S., Wu, S., et al. (2008). Biogenic versus anthropogenic sources of CO in the United States. *Geophysical Research Letters*, *35*(4), 1–5. https://doi.org/10.1029/2007GL032393

Jiang, Z., Jones, D. B. A., Kopacz, M., Liu, J., Henze, D. K., & Heald, C. (2011). Quantifying the impact of model errors on top-down estimates of carbon monoxide emissions using satellite observations. *Journal of Geophysical Research*, *116*, D15306. https://doi.org/10.1029/2010JD015282

Jiang, Z., Jones, D. B. A., Worden, H. M., Deeter, M. N., Henze, D. K., Worden, J., et al. (2013). Impact of model errors in convective transport on CO source estimates inferred from MOPITT CO retrievals. *Journal of Geophysical Research: Atmospheres*, *118*, 2073–2083. https://doi.org/10.1002/jgrd.50216

Jiang, Z., Worden, J. R., Jones, D. B. A., Lin, J. T., Verstraeten, W. W., & Henze, D. K. (2015). Constraints on Asian ozone using Aura TES, OMI and Terra MOPITT. *Atmospheric Chemistry and Physics*, *15*(1), 99–112. https://doi.org/10.5194/acp-15-99-2015

Joiner, J., Guanter, L., Lindstrot, R., Voigt, M., Vasilkov, A. P., Middleton, E. M., et al. (2013). Global monitoring of terrestrial chlorophyll fluorescence from moderate-spectral-resolution near-infrared satellite measurements: Methodology, simulations, and application to GOME-2. *Atmospheric measurement techniques*, *6*(10), 2803–2823. https://doi.org/10.5194/amt-6-2803-2013

Jung, M., Reichstein, M., Margolis, H. A., Cescatti, A., Richardson, A. D., Arain, M. A., et al. (2011). Global patterns of land-atmosphere fluxes of carbon dioxide, latent heat, and sensible heat derived from eddy covariance, satellite, and meteorological observations. *Journal of Geophysical Research*, *116*(3), 1–16. https://doi.org/10.1029/2010JG001566

Kettle, A. J., Kuhn, U., von Hobe, M., Kesselmeier, J., & Andreae, M. O. (2002). Global budget of atmospheric carbonyl sulfide: Temporal and spatial variations of the dominant sources and sinks. *Journal of Geophysical Research*, *107*, 4658. https://doi.org/10.1029/2002jd002187

Kopacz, M., Jacob, D. J., Fisher, J. A., Logan, J. A., Zhang, L., Megretskaia, I. A., et al. (2010). Global estimates of CO sources with high resolution by adjoint inversion of multiple satellite datasets (MOPITT, AIRS, SCIAMACHY, TES). *Atmospheric Chemistry and Physics*, *10*, 855–876. https://doi.org/10.5194/acp-10-855-2010

Kopacz, M., Jacob, D. J., Henze, D. K., Heald, C. L., Streets, D. G., & Zhang, Q. (2009). Comparison of adjoint and analytical Bayesian inversion methods for constraining Asian sources of carbon monoxide using satellite (MOPITT) measurements of CO columns. *Journal of Geophysical Research*, *114*, D04305. https://doi.org/10.1029/2007JD009264

Kuhns, H., Green, M., & Etyemezian, V. (2003). *Big bend regional aerosol and visibility observational (BRAVO) study emissions inventory, report prepared for BRAVO steering committee*. Nevada: Desert Research Institute, Las Vegas.

Liu, J., Baskaran, L., Bowman, K., Schimel, D., Bloom, A. A., Parazoo, N. C., et al. (2020). Carbon monitoring system flux net biosphere exchange 2020 (CMS-Flux NBE 2020). *Earth System Science Data Discussions*, 1–53.

Liu, J., Bowman, K., Lee, M., Henze, D., Bousserez, N., Brix, H., et al. (2014). Carbon monitoring system flux estimation and attribution: Impact of ACOS-GOSAT XCO2 sampling on the inference of terrestrial biospheric sources and sinks. *Tellus B: Chemical and Physical Meteorology*, *66*, 22486. https://doi.org/10.3402/tellusb.v66.22486

Liu, J., Wennberg, P. O., Parazoo, N. C., Yin, Y., & Frankenberg, C. (2020). Observational constraints on the response of high - latitude northern forests to warming. *AGU Advances*, *1*(4), e2020AV000228. https://doi.org/10.1029/2020av000228

Liu, L., Zhuang, Q., Zhu, Q., Liu, S., Asperen, H. V., & Pihlatie, M. (2018). Global soil consumption of atmospheric carbon monoxide: An analysis using a process-based biogeochemistry model. *Atmospheric Chemistry and Physics*, *18*(11), 7913–7931. https://doi.org/10.5194/acp-18-7913-2018

Lokupitiya, E., Denning, S., Paustian, K., Baker, I., Schaefer, K., Verma, S., et al. (2009). Incorporation of crop phenology in simple biosphere model (SiBcrop) to improve land-atmosphere carbon exchanges from croplands. *Biogeosciences*, *6*, 969–986. https://doi.org/10.5194/bg-6-969-2009

Ma, J., Kooijmans, L. M., Cho, A., Montzka, S. A., Glatthor, N., Worden, J. R., et al. (2021). Inverse modelling of carbonyl sulfide: Implementation, evaluation and implications for the global budget. *Atmospheric Chemistry and Physics*, *21*(5), 3507–3529.

Madani, N., Parazoo, N. C., Kimball, J. S., Ballantyne, A. P., Saatchi, S., Palmer, P. I., et al. (2020). Amplified global gross primary productivity due to temperature increase is offset by reduced productivity due to water constraint. *AGU Advances*, *1*(4), e2020AV000180. https://doi.org/10.1029/2020av000180

Magney, T. S., Barnes, M. L., & Yang, X. (2020). On the covariation of chlorophyll fluorescence and photosynthesis across scales. *Geophysical Research Letters*, *47*(23), 1–7. https://doi.org/10.1029/2020gl091098

Martínez-Alonso, S., Deeter, M., Worden, H., Borsdorff, T., Aben, I., Commane, R., et al. (2020). 1.5 years of TROPOMI CO measurements: Comparisons to MOPITT and ATom. *Atmospheric Measurement Techniques*, *13*(9), 4841–4864. https://doi.org/10.5194/amt-13-4841-2020

Michalak, A. M. (2004). A geostatistical approach to surface flux estimation of atmospheric trace gases. *Journal of Geophysical Research*, *109*(D14), D14109. https://doi.org/10.1029/2003jd004422

Miles, N. L., Richardson, S. J., Davis, K. J., Lauvaux, T., Andrews, A. E., West, T. O., et al. (2012). Large amplitude spatial and temporal gradients in atmospheric boundary layer CO_2 mole fractions detected with a tower-based network in the U.S. upper Midwest. *Journal of Geophysical Research*, *117*, G01019. https://doi.org/10.1029/2011JG001781

Miles, N. L., Richardson, S. J., Martins, D. K., Davis, K. J., Lauvaux, T., Haupt, B. J., & Miller, S. K. (2018). *ACT-America: L2 in situ CO_2, CO, and CH_4 concentrations from towers, eastern USA*. Oak Ridge, Tennessee, USA: ORNL DAAC. https://doi.org/10.3334/ORNLDAAC/1568

Miller, J. B., Lehman, S. J., Verhulst, K. R., Miller, C. E., Duren, R. M., Yadav, V., & Sloop, C. D. (2020). Large and seasonally varying biospheric CO_2 fluxes in the Los Angeles megacity revealed by atmospheric radiocarbon. *Proceedings of the National Academy of Sciences of the United States of America*, *117*(43), 26681–26687. https://doi.org/10.1073/pnas.2005253117

Miyazaki, K., Bowman, K. W., Yumimoto, K., Walker, T., & Sudo, K. (2020). Evaluation of a multi-model, multi-constituent assimilation framework for tropospheric chemical reanalysis. *Atmospheric Chemistry and Physics*, *20*(2), 931–967. https://doi.org/10.5194/acp-20-931-2020

Nakanishi, M., & Niino, H. (2004). An improved Mellor-Yamada Level-3 model with condensation physics: Its design and verification. *Boundary-Layer Meteorology*, *112*, 1–31. https://doi.org/10.1023/B:BOUN.0000020164.04146.98

Nehrkorn, T., Eluszkiewicz, J., Wofsy, S. C., Lin, J. C., Gerbig, C., Longo, M., & Freitas, S. (2010). Coupled weather research and forecasting–stochastic time-inverted lagrangian transport (WRF–STILT) model. *Meteorology and Atmospheric Physics*, *107*(1–2), 51–64. https://doi.org/10.1007/s00703-010-0068-x

Oda, T., Maksyutov, S., & Andres, R. J. (2018). The open-source data inventory for anthropogenic carbon dioxide (CO_2), version 2016 (ODIAC2016): A global, monthly fossil-fuel CO_2 gridded emission data product for tracer transport simulations and surface flux inversions. *Earth System Science Data*, *10*(1), 87–107. https://doi.org/10.5194/essd-10-87-2018

Olivier, J. G. J., & Berdowski, J. J. M. (2001). Global emissions sources and sinks. In J. Berdowski, R. Guicherit, B. J. Heij, & A. A. Balkema (Eds.), The Climate System (Vol. 33–78). Lisse, the Netherlands: Publishers/Swets & Zeitlinger Publishers.

Olsen, S. C., & Randerson, J. T. (2004). Differences between surface and column atmospheric CO_2 and implications for carbon cycle research. *Journal of Geophysical Research*, *109*, D02301. https://doi.org/10.1029/2003jd003968

Parazoo, N. C., Bowman, K., Fisher, J. B., Frankenberg, C., Jones, D. B. A., Cescatti, A., et al. (2014). Terrestrial gross primary production inferred from satellite fluorescence and vegetation models. *Global Change Biology*, *20*(10), 3103–3121. https://doi.org/10.1111/gcb.12652

Parazoo, N. C., Commane, R., Wofsy, S. C., Koven, C. D., Sweeney, C., Lawrence, D. M., et al. (2016). Detecting regional patterns of changing CO_2 flux in Alaska. *Proceedings of the National Academy of Sciences of the United States of America*, *113*(28), 7733–7738. https://doi.org/10.1073/pnas.1601085113

Parazoo, N. C., Denning, A. S., Kawa, S. R., Pawson, S., & Lokupitiya, R. (2012). CO_2 flux estimation errors associated with moist atmospheric processes. *Atmospheric Chemistry and Physics*, *12*, 6405–6416. https://doi.org/10.5194/acp-12-6405-2012

Parazoo, N. C., Magney, T., Baker, I., Raczka, B., Bacour, C., Maignan, F., et al. (2020). Wide discrepancies in the magnitude and direction of modelled SIF in response to light conditions. *Biogeosciences*, *17*(13), 3733–3755. https://doi.org/10.5194/bg-17-3733-2020

Parrington, M., Jones, D. B. A., Bowman, K. W., Horowitz, L. W., Thompson, A. M., Tarasick, D. W., & Witte, J. C. (2008). Estimating the summertime tropospheric ozone distribution over North America through assimilation of observations from the tropospheric emission spectrometer. *Journal of Geophysical Research*, *113*, D18307. https://doi.org/10.1029/2007JD009341

Peters, W., Jacobson, A. R., Sweeney, C., Andrews, A. E., Conway, T. J., Masarie, K., et al. (2007). An atmospheric perspective on North American carbon dioxide exchange: CarbonTracker. *Proceedings of the National Academy of Sciences of the United States of America*, *104*(48), 18925–18930. https://doi.org/10.1073/pnas.0708986104

Raczka, B., Porcar-Castell, A., Magney, T., Lee, J. E., Köhler, P., Frankenberg, C., et al. (2019). Sustained nonphotochemical quenching shapes the seasonal pattern of solar-induced fluorescence at a high-elevation evergreen forest. *Journal of Geophysical Research: Biogeosciences*, *124*(7), 2005–2020. https://doi.org/10.1029/2018JG004883

Runkle, B. R. K., Rigby, J. R., Reba, M. L., Anapalli, S. S., Bhattacharjee, J., Krauss, K. W., et al. (2017). Delta-Flux: An eddy covariance network for a climate-smart Lower Mississippi Basin. *Agricultural & Environmental Letters*, *2*, 170003. https://doi.org/10.2134/ael2017.01.0003

Schaefer, K., Collatz, G. J., Tans, P., Denning, A. S., Baker, I., Berry, J., et al. (2008). Combined simple biosphere/carnegie-ames-stanford approach terrestrial carbon cycle model. *Journal of Geophysical Research*, *113*, G03034. https://doi.org/10.1029/2007JG000603

Schaefer, K., Zhang, T., Slater, A. G., Lu, L., Etringer, A., & Baker, I. (2009). Improving simulated soil temperatures and soil freeze/thaw at high-latitude regions in simple biosphere/carnegie-ames-stanford approach model. *Journal of Geophysical Research*, *114*, F02021. https://doi.org/10.1029/2008JF001125

Schimel, D., Stephens, B. B., & Fisher, J. B. (2015). Effect of increasing CO_2 on the terrestrial carbon cycle. *Proceedings of the National Academy of Sciences of the United States of America*, *112*(2), 436–441. https://doi.org/10.1073/pnas.1407302112

Schuh, A. E., Jacobson, A. R., Basu, S., Weir, B., Baker, D., Bowman, K., et al. (2019). Quantifying the impact of atmospheric transport uncertainty on CO_2 surface flux estimates. *Global Biogeochemical Cycles*, *33*(4), 484–500. https://doi.org/10.1029/2018gb006086

Schuh, A. E., Lauvaux, T., West, T., Scott Denning, A., Davis, K. J., Miles, N., et al. (2013). Evaluating atmospheric CO_2 inversions at multiple scales over a highly-inventoried agricultural landscape. *Global Change Biology*, *9*, 1424–1439. https://doi.org/10.1111/gcb.12141

Shiga, Y. P., Tadić, J. M., Qiu, X., Yadav, V., Andrews, A. E., Berry, J. A., & Michalak, A. M. (2018). Atmospheric CO_2 observations reveal strong correlation between regional net biospheric carbon uptake and solar-induced chlorophyll fluorescence. *Geophysical Research Letters*, *45*(2), 1122–1132. https://doi.org/10.1002/2017gl076630

Sitch, S., Friedlingstein, P., Gruber, N., Jones, S. D., Murray-Tortarolo, G., Ahlström, A., et al. (2015). Recent trends and drivers of regional sources and sinks of carbon dioxide. *Biogeosciences*, *12*(3), 653–679. https://doi.org/10.5194/bg-12-653-2015

Stein, A. F., Draxler, R. R., Rolph, G. D., Stunder, B. J., Cohen, M. D., & Ngan, F. (2015). NOAA's HYSPLIT atmospheric transport and dispersion modeling system. *Bulletin of the American Meteorological Society*, *96*(12), 2059–2077. https://doi.org/10.1175/bams-d-14-00110.1

Stephens, B. B., Gurney, K. R., Tans, P. P., Sweeney, C., Peters, W., Bruhwiler, L., et al. (2007). Weak northern and strong tropical land carbon uptake from vertical profiles of atmospheric CO_2. *Science*, *316*(5832), 1732–1735. https://doi.org/10.1126/science.1137004

Stimler, K., Berry, J. A., Montzka, S. A., & Yakir, D. (2011). Association between carbonyl sulfide uptake and 18Δ during gas exchange in C3 and C4 leaves. *Plant Physiology*, *157*(1), 509–517. https://doi.org/10.1104/pp.111.176578

Stinecipher, J. R., Cameron-Smith, P. J., Blake, N. J., Kuai, L., Lejeune, B., Mahieu, E., et al. (2019). Biomass burning unlikely to account for missing source of carbonyl sulfide. *Geophysical Research Letters*, *46*(24), 14912–14920. https://doi.org/10.1029/2019gl085567

Stöckli, R., Rutishauser, T., Baker, I., Liniger, M. A., & Denning, A. S. (2011). A global reanalysis of vegetation phenology. *Journal of Geophysical Research*, *116*(G3), G03020. https://doi.org/10.1029/2010jg001545

Stöckli, R., Rutishauser, T., Dragoni, D., O'Keefe, J., Thornton, P. E., Jolly, M., et al. (2008). Remote sensing data assimilation for a prognostic phenology model. *Journal of Geophysical Research*, *113*(G4), G04021. https://doi.org/10.1029/2008JG000781

Stöckli, R., & Vidale, P. L. (2005). Modeling diurnal to seasonal water and heat exchanges at European Fluxnet sites. *Theoretical and Applied Climatology*, *80*(2–4), 229–243. https://doi.org/10.1007/s00704-004-0102-3

Sweeney, C., Karion, A., Wolter, S., Newberger, T., Guenther, D., Higgs, J. A., et al. (2015). Seasonal climatology of CO_2 across North America from aircraft measurements in the NOAA/ESRL Global Greenhouse Gas Reference Network. *Journal of Geophysical Research: Atmospheres*, *120*(10), 5155–5190. https://doi.org/10.1002/2014jd022591

van der Werf, G. R., Randerson, J. T., Giglio, L., Collatz, G. J., Mu, M., Kasibhatla, P. S., et al. (2010). Global fire emissions and the contribution of deforestation, savanna, forest, agricultural, and peat fires (1997– 2009). *Atmospheric Chemistry and Physics*, *10*, 11707–11735. https://doi.org/10.5194/acp-10-11707-2010

Wang, W., Dwivedi, P., Abt, R., & Khanna, M. (2015). Carbon savings with transatlantic trade in pellets: Accounting for market-driven effects. *Environmental Research Letters*, *10*(11), 114019. https://doi.org/10.1088/1748-9326/10/11/114019

Wei, Y., Shrestha, R., Pal, S., Gerken, T., McNelis, J., Singh, D., et al. (2021). The Atmospheric Carbon and Transport (ACT) – America datasets: Description, management, and delivery. *Earth and Space Science*, *8*(7), e2020EA001634. https://doi.org/10.1029/2020ea001634

Whelan, M. E., Anderegg, L. D. L., Badgley, G., Campbell, J. E., Commane, R., Frankenberg, C., et al. (2020). Scientific communities striving for a common cause: Innovations in carbon cycle science. *Bulletin of the American Meteorological Society*, *101*(9), E1537–E1543. https://doi.org/10.1175/bams-d-19-0306.1

Whelan, M. E., Hilton, T. W., Berry, J. A., Berkelhammer, M., Desai, A. R., & Campbell, J. E. (2016). Carbonyl sulfide exchange in soils for better estimates of ecosystem carbon uptake. *Atmospheric Chemistry and Physics*, *16*(6), 3711–3726. https://doi.org/10.5194/acp-16-3711-2016

Whelan, M. E., Min, D. H., & Rhew, R. C. (2013). Salt marsh vegetation as a carbonyl sulfide (COS) source to the atmosphere. *Atmospheric Environment*, *73*, 131–137. https://doi.org/10.1016/j.atmosenv.2013.02.048

Worden, H. M., Bloom, A. A., Worden, J. R., Jiang, Z., Marais, E. A., Stavrakou, T., et al. (2019). New constraints on biogenic emissions using satellite-based estimates of carbon monoxide fluxes. *Atmospheric Chemistry and Physics*, *19*, 13569–13579. https://doi.org/10.5194/acp-19-13569-2019

Yin, Y., Byrne, B., Liu, J., Wennberg, P., Davis, K. J., Magney, T., et al. (2020). Cropland carbon uptake delayed and reduced by 2019 Midwest floods. *AGU Advances*, *1*, e2019AV000140. https://doi.org/10.1029/2019AV000140

Zumkehr, A., Hilton, T. W., Whelan, M., Smith, S., Kuai, L., Worden, J., & Campbell, J. E. (2018). Global gridded anthropogenic emissions inventory of carbonyl sulfide. *Atmospheric Environment*, *183*, 11–19. https://doi.org/10.1016/j.atmosenv.2018.03.063

Reference From the Supporting Information

Still, C. J., Berry, J. A., Collatz, G. J., & DeFries, R. S. (2003). Global distribution of C3 and C4 vegetation: Carbon cycle implications. *Global Biogeochemical Cycles*, *17*(1), 6–1. https://doi.org/10.1029/2001gb001807